PHOTONICS

Detail of an array of silicon dioxide recesses filled by GaAs devices. Image by Fonstad group.

TABLE OF CONTENTS

Excitons in Organic Optoelectronic Devices

C. Madigan, V. Bulovic

Most of the published physical studies on disordered molecular organic materials investigate charge conduction mechanisms, specifically the microscopic and macroscopic behavior of polarons. While consensus remains elusive, in part because of the continuing uncertainty over the role of interfaces as compared to the bulk in determining device performance, there has been considerable progress. By comparison, very few studies have been published on exciton dynamics in organic optoelectronic devices (where excitons are the dominant optical excitations in amorphous organic materials). Exciton modeling studies are often qualitative, reduced to parameters such as the exciton diffusion length and exciton lifetime, leaving significant questions unanswered about the detailed microscopic processes and how to develop models capable of yielding quantitative device properties on the macro-scale.

In this project, we aim to develop detailed exciton dynamics models to enable and implement device-level simulations. Three considerations motivate this work. First, as has long been recognized in the inorganic semiconductor industry, designing a device on paper and simulating it using a computer is far more efficient than designing, fabricating and testing a device. Second, good models of both polarons and excitons are necessary to accurately simulate optoelectronic device behavior, but at this stage, comparatively little attention has been given to excitons. Finally, since few studies simultaneously consider polaron and exciton simulations to treat the behavior of these devices, it is significant to determine the specific ways to efficiently and accurately combine existing models of polarons with improved models of excitons in a combined simulation.

To date, we demonstrated that exciton energy levels are altered through interaction with neighboring molecules by the mechanism of solid-state solvation. We continue to investigate other electric-field-induced, excitonic energy-level shifts. We have also demonstrated that ultra-fast, time-resolved, fluorescence spectroscopy can be used to probe exciton diffusion in our materials, as previously demonstrated for polymer films. We have developed a complete Monte Carlo simulation of exciton diffusion in disordered molecular solids by treating spatial and energetic disorder and diffusion by either Dexter or Forster energy transfer. This simulation models homogenous, continuous solids as well as doped and structured materials, as required for treating devices. Existing analytical models for treating the general excitation diffusion in disordered media have been evaluated and found to be generally inapplicable to this project. Current work develops additional experimental methods for monitoring exciton diffusion, namely site-selective fluorescence and fluorescence-polarization anisotropy, and modifyies the exciton Monte Carlo simulation to incorporate polarons.
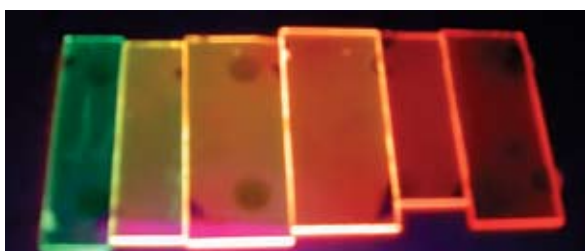
Figure 1: Series of DCM2:AlQ3 fluorescing films showing DCM2 excitonic energy shifts (i.e., different colors) due to intermolecular interactions. The leftmost film shows AlQ3 PL, and the remaining films show DCM2 PL for different DCM2 dopings.
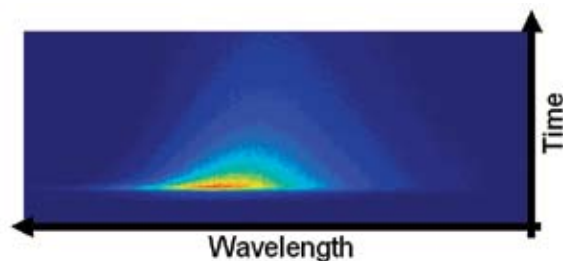
Figure 2: Example of ultra-fast, time-resolved, fluorescence data. The vertical axis denotes wavelength; the horizontal axis, time. In this example, DCM2 is the photo-luminescing material, doped into an AlQ3 host.

Layer-by-Layer, J-aggregate Thin Films with an Absorption Constant of 10^6 cm^{-1} in Optoelectronic Applications

J.R. Tischler, M.S. Bradley, V. Bulovic
Sponsorship: DARPA Optocenter, NDSEG, NSF-MRSEC

Thin films of J-aggregate cyanine dyes deposited by layer-by-layer (LBL) assembly exhibit exciton-polariton dynamics when incorporated in an optical microcavity. Such LBL, J-aggregate thin films can be precisely deposited in a specific location in an optical microcavity, enabling the development of previously unachievable optoelectronic devices, as for example, the recently demonstrated resonant-cavity exciton-polariton organic light-emitting device [1].

To gain insight into the physical properties of these films, we investigate the optical and morphological properties of 5,6-dichloro-2-[3-[5,6-dichloro-1-ethyl-3-(3-sulfopropyl)-2(3H)-benzimidazolidene]-1-propenyl]-1-ethyl-3-(3-sulfopropyl) benzimidazolium hydroxide, inner salt, sodium salt (TDBC) J-aggregates, alternately adsorbed with poly-(diallyldimethylammonium chloride) (PDAC) on glass substrates. Atomic force microscopy (AFM) shows that the first few sequential immersions in cationic and anionic solutions (SICAS) form layered structures, which give way to Stransky-Krastanov-type growth in subsequent SICAS. We combine thickness measurements from AFM and spectroscopic data to determine the optical constants of the films and find that at the peak absorption wavelength of 596 nm, the films possess an absorption coefficient of $\alpha = 1.05 \pm 0.1 \times 10^6$ cm^{-1}, among the highest ever measured for a neat thin film. The optical constants were calculated by fitting spectroscopic data for films in the layered growth regime to a model based on propagation and matching matrices (Figure 1).

The presented method is a general approach to generating thin films with very large absorption constant, an enabling step in the fabrication of novel devices that utilize strong coupling of light and matter, such as light emitting devices (Figure 2) and polariton lasers.
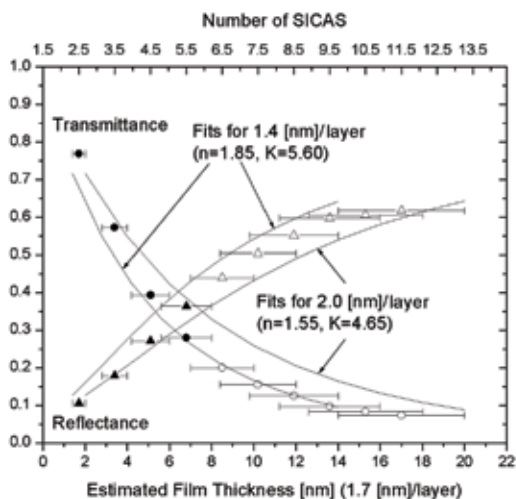
Figure 1: Optical data plotted with a least-squared-error fit for the optical constants at λ=596 nm using a model of propagation and matching matrices. The filled versus outlined points are for samples where layered versus Stransky-Krastanov growth dominate, respectively. The filled points were used for the least-squared-error fit.
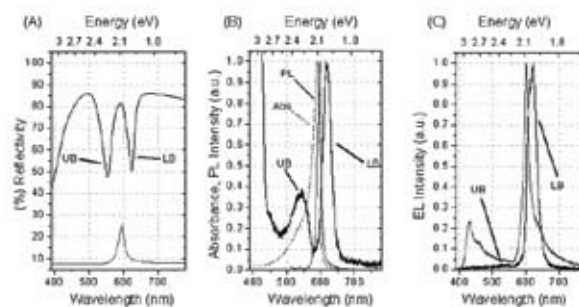
Figure 2: Reflectivity, photoluminescence, and electroluminescence of a single polariton, resonant-cavity, organic light-emitting device with microcavity closely tuned to the J-aggregate resonance.

REFERENCES:

[1]   Tischler, J.R., M.S. Bradley, V. Bulovic, J.H. Song, A. Nurmikko, "Strong Coupling in a Microcavity LED", *Phys. Rev. Lett.* (2005).

Patterned Quantum Dot Monolayers in QD-LEDs

S. Coe-Sullivan, L. Kim, J. Steckel, R. Tabone, M.G. Bawendi, V. Bulovic
Sponsorship: Presidential Early Career Award for Scientists and Engineers, ISN, NSF-MRSEC, Deshpande Center

Hybrid organic/inorganic quantum dot light-emitting devices (QD-LEDs) contain luminescent nanocrystal quantum dots (QDs) imbedded in an organic thin film structure. The QDs are nanometer-size particles of inorganic semiconductors that exhibit efficient luminescence; their emission colors can be tuned by changing the size of the nanocrystals. For example, the luminescence of QDs of CdSe is tuned from blue to red by changing the QD diameter from 2nm to 12nm. By further changing the material system, saturated color emission can be tuned from the UV, through the visible, and into the IR. The inorganic emissive component provides potential for a long operating lifetime of QD-LEDs. The room temperature fabrication method ensures compatibility of the QD-LED technology with the established all-organic LEDs (OLEDs).

The optimized QD-LED device structure contains a single monolayer of QDs embedded within the layered, organic thin-film structure. The technology is enabled by the self-assembly of the QDs as a densely packed monolayer on top of a conjugated organic film. The QD film is positioned with nanometer precision in the recombination zone of the device [1]. Most recently, by using a microcontact printing (stamping) process, we demonstrated that neat layers of QDs can be placed independently of the organic layers and in-plane patterned, allowing for the pixel formation necessary for display technology (Figure 1). To date, we demonstrated QD-LED color emission across the visible part of the spectrum and from 1.3µm to 1.6µm in the near infra-red (Figure 2).
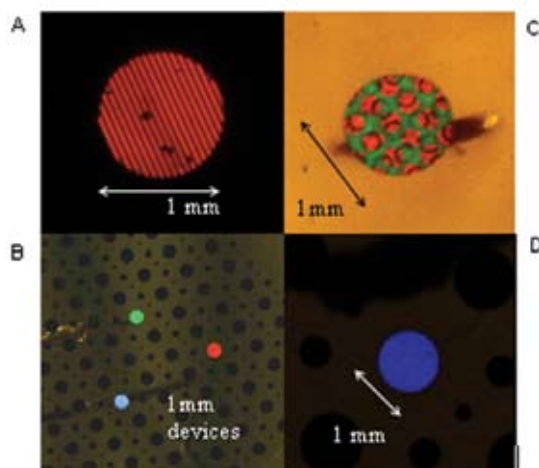
Figure 1: (A) A 25-um-wide, lined, red QD-LED, patterned by microcontact printing (stamping). (B) Stamped red QD-LED, stamped green QD-LED, and blue organic LED. (C) Stamped, patterned, green/red QD-LED. (D) Stamped blue QD-LED.
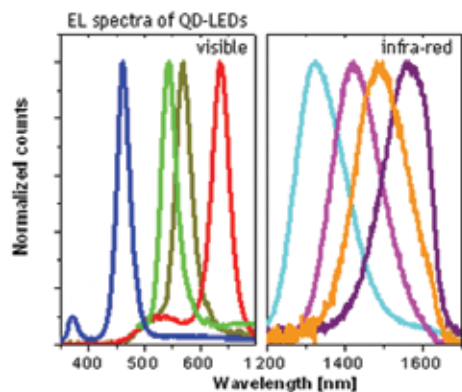
Figure 2: Electroluminescence spectra of QD-LEDs in visible and infra-red.

REFERENCES:

[1]   Coe-Sullivan, S., W. Woo, J. Steckel, M.G. Bawendi, V. Bulovic, "Tuning the Performance of Hybrid Organic/Inorganic Quantum Dot Light-Emitting Devices," *Organic Electronics* 4, 123 (2003).

Quantum Dot Light-Emitting Devices

S. Coe-Sullivan, P. Anikeeva, J. Steckel, M. Bawendi, V. Bulovic

Hybrid organic/inorganic light-emitting devices (QD-LEDs) combine stability and color clarity of semiconductor nanoparticles and low-cost processing procedures of organic materials with the aim to generate a flat-panel-display technology. Semiconductor quantum dots (QDs) are nanocrystals that are of smaller diameter than the Bohr exciton in a bulk crystal of the same material. By reducing the size of the nanocrystal, quantum confinement effects lead to an increase in the band-edge, exciton energy. Changing QD sizes and materials can produce luminescence wavelength from UV, trough visible spectrum, and near-IR.

A typical QD-LED consists of a transparent inorganic anode deposited on a glass substrate followed by organic electron (ETL) and hole transport layers (HTL) with a QD monolayer in between. A metal cathode is deposited on top of the structure as Figures 1 and 2 (left) show. We are presently investigating physical mechanisms that govern light generation in QD-LEDs. Time-resolved optical methods allow us to study charge and exciton transport in organic films and at organic/QD interfaces, as in Figure 2 (right). Physical insights lead to an optimized design and improved performance of QD-LEDs.
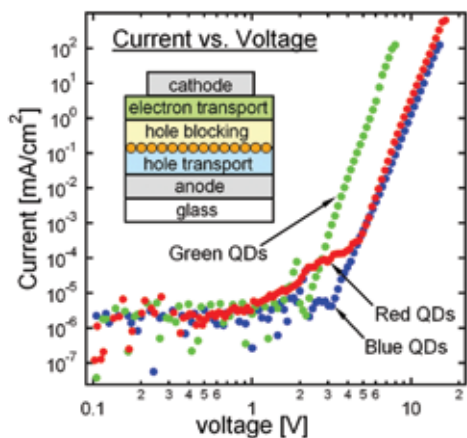
Figure 1: Current-Voltage (IV) characteristics of QD-LEDs with monolayers of red, green, and blue QDs as the recombination layers. Top left corner:structure of the device.
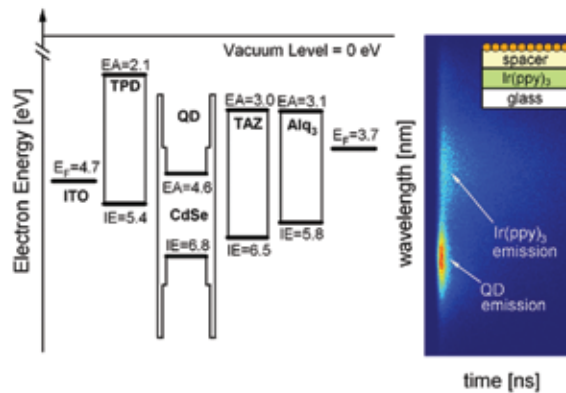
Figure 2: On the left: level diagram of a typical QD-LED. On the right: time-resolved photoluminescence measurement of the structure on the top right corner.

Development of Terahertz Quantum-Cascade Lasers

B. Williams, H. Callebaut, S. Kumar, S. Kohen, Q. Hu, in collaboration with Dr. J. Reno (Sandia National Lab)

The terahertz frequency range (1-10 THz) has long remained undeveloped, mainly due to the lack of compact, coherent radiation sources. Transitions between subbands in semiconductor quantum wells were suggested as a method to generate long-wavelength radiation at customizable frequencies. However, because of difficulties in achieving population inversion between narrowly separated sub-bands and mode confinement at long wavelengths, THz lasers based on intersubband transitions were developed only very recently. Taking a completely novel approach, we have developed THz quantum-cascade lasers based on resonant-phonon-assisted depopulation and using metal-metal waveguides for mode confinement. The schematics of both features are illustrated in Figure 1. Combining these two unique features, we have developed many THz QCLs with record performance, including a maximum-pulsed-operating temperature at 164 K (Figure 2), a maximum-cw-operating temperature at 117 K (Figure 3), and the longest wavelength (~141µm) QCL to date without the assistance of magnetic fields (Figure 4).
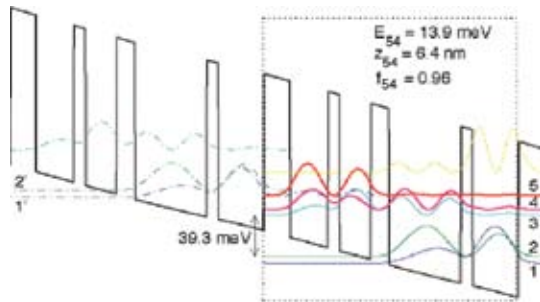
Figure 1
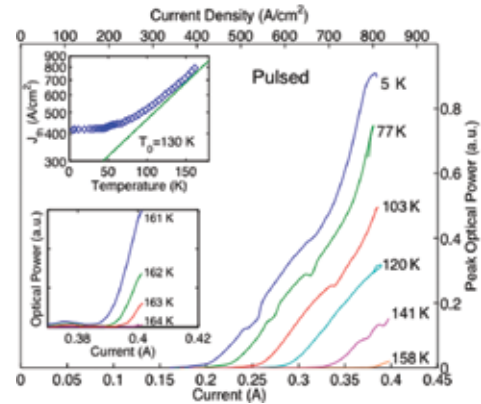
Figure 2
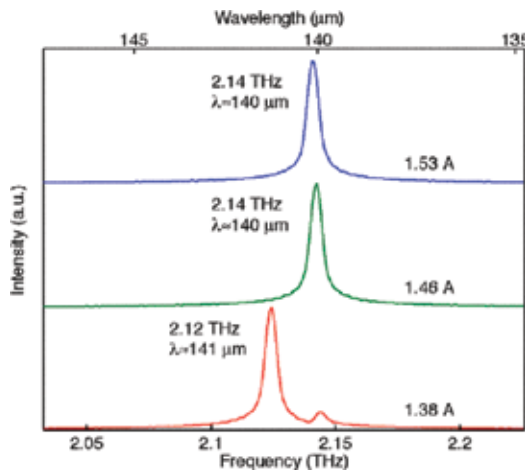
Figure 3
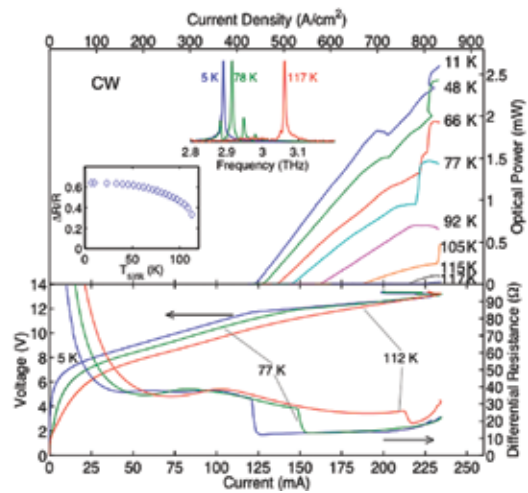
Figure 4

Broadband, Saturable, Bragg Reflectors for Mode-locking, Ultrafast Lasers

S. Tandon, J. Gopinath, H. Shen, G. Petrich, F. Kaertner, E. Ippen, L. Kolodziejski
Sponsorship: ONR MURI

Broadband Saturable Bragg Reflectors (SBR) consisting of monolithically integrated absorbers onto GaAs-based Bragg-mirrors have been used in a variety of ultra-short pulse lasers. The absorber, high-index layers and layer thicknesses are selected based on the laser's wavelength. In contrast, the low-index layer is always Al_xO_y that was created by the wet oxidation of AlAs layers. Reflectivity measurements of a variety of fabricated SBRs are shown in Figure 1.

Infrared SBRs are composed of AlGaAs/Al_xO_y mirrors with InGaAs-based absorbers which strain the structure and, depending on the absorber thickness, may lead to delamination during the AlAs oxidation process. Figure 2(a) shows a plan view of a fully oxidized 500μm diameter SBR that is designed for operation at λ=1230nm. The cross-sectional view (Figure 2(b)) shows the delaminated absorber consisting of the highly strained 80nm thick InGaAs quantum well with GaAs cladding layers and a 7-pair $Al_{0.3}Ga_{0.7}As$/Al_xO_y mirror stack. For oxidation temperatures between 410°C and 435°C, delamination occurs between the absorber and mirror layers. More severe delamination occurs at higher oxidation temperatures. In an alternate SBR design, the additional strain introduced by the InP cladding layers generally increases the observed amount of delamination. A controlled temperature ramp before and after oxidation has greatly reduced the delamination of the SBR structures despite the presence of strain.

The same AlAs oxidation technique also enables the fabrication of visible SBRs. Using $In_{0.5}Ga_{0.15}Al_{0.35}P$ as the high-index layer and Al_xO_y, Bragg mirrors are created for operation below 800 nm. Along with a GaAs absorber layer, these visible SBRs are nominally unstrained and may mode-lock a variety of lasers including Ti:Sapphire, Cr:LiSAF, Cr:LiCAF, and Cr:LiSGaF. Figures 2(c) and 2(d) show a plan view and a cross-sectional view of one such SBR.
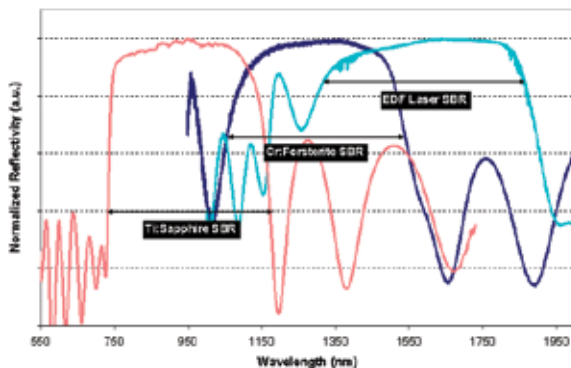
Figure 1: Reflectivity measurements of SBR structures fabricated for three different laser systems: Ti:Sapphire, Cr:Forsterite, and Er-doped fiber (EDF) laser. The Ti:Sapphire SBR was measured with a microspectrophotometer (courtesy of Filmetrics, Inc.). SBRs for the Cr:Forsterite and EDF lasers were measured using Fourier Transform Infrared Spectroscopy.
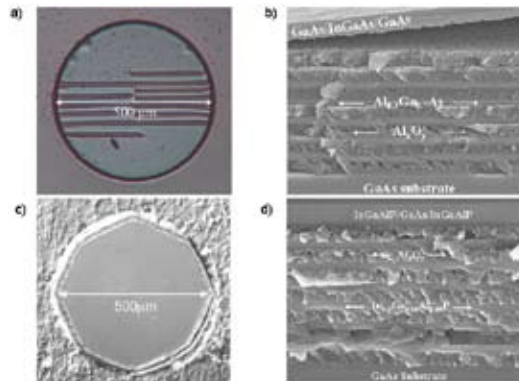
Figure 2: a) Differential Interference Contrast (DIC) image of a fully-oxidized infrared SBR. b) Cross-sectional SEM image showing delamination of the absorber layers from the mirror stack. c) DIC image of fully-oxidized visible SBR. d) Cross-sectional SEM image showing the GaAs-based absorber with a 7 pair InGaAlP/Al_xO_y mirror stack.

Approaching the InP-Lattice Constant on GaAs

N.J. Quitoriano, E.A. Fitzgerald
Sponsorship: Walsin Lihwa

Integrating different materials onto the Si platform brings new functionality to silicon. Using InP on silicon could allow the integration of optical and electronic (e.g., CMOS) devices. By growing high-quality GaAs on silicon, our group has been able to demonstrate a GaAs laser on silicon. Our research goal is to expand the lattice constant beyond GaAs and grow high-quality InP on GaAs. Having explored many materials systems and methods (e.g., InGaAs, InGaP, and InGaAlAs), to date, we have grown low-dislocation-density $In_{(0.43)}Al_{(0.57)}As$ on GaAs with a dislocation density of 1.4E6/cm^2, more than an order-of-magnitude fewer dislocations than in typical commercial metamorphic buffers. After achieving high-quality InP on GaAs, we will work to grow InP on Si. Bringing low-defect density InP onto Si may bring high-speed, InP-based devices into new markets because the processing and material-cost, for a given area will be drastically reduced and allow for high-frequency and/or low-power operation.

Figure 1: Plan-view TEM of $In_{(0.43)}Al_{(0.57)}As$ on GaAs with a dislocation density of 1.4E6/cm^2.
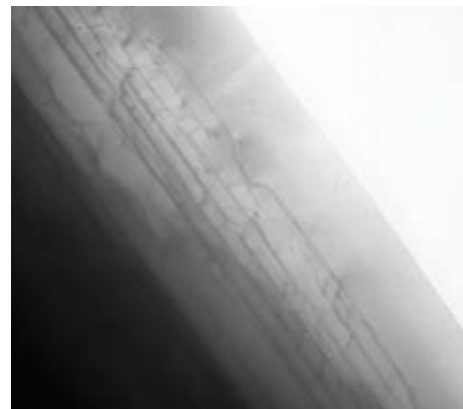
Figure 2: Cross-section of $In_{(0.43)}Al_{(0.57)}As$ on GaAs.

Growth and Characterization of High Quality Metamorphic Quantum Well Structure on GaAs

H.K.H. Choy, C.G. Fonstad, Jr
Sponsorship: Charles Stark Draper Laboratory, NSF

A potentially useful technique to extend the emission wavelength of quantum well (QW) lasers on GaAs substrates is to fabricate the laser structures metamorphically on compositionally graded InGaAs buffers. In such buffers, the indium fraction is increased gradually as growth proceeds. This results in steady elongation of the existing dislocations along the growth surface, releasing the additional strain, and the density of threading dislocations can be minimized. Mismatched metamorphic materials have been grown with the use of graded buffers for over 30 years and the most notable successes are mainly in electronic applications, such as InGaAs HEMTs on GaAs, and strained Si or SiGe high mobility MOSFETs on Si. The adaptation of graded buffers to optoelectronic devices, on the contrary, has been much slower, and we have been working to change this situation.

We have recently demonstrated that the use of *ex-situ* thermal annealing can yield a 30-fold improvement in the photoluminescence (PL) of aluminum-containing single QW structures grown on top of compositionally graded InGaAs buffers [1]. By analyzing the variations of low temperature PL from both the barriers and from the QW as functions of the annealing temperatures, as shown in Figure 1, we have concluded that two processes are involved in the annealing process: a faster one in the barriers and a much slower one in the QW region. By annealing diode structures on the graded buffers, we also observed a large increase in the reverse-biased breakdown voltage from $\approx 0V$, due to tunneling through the mid-gap states, to 23V: the avalanche breakdown voltage of the diodes, as Figure 2 shows. Additional QW PL enhancement is found by annealing the samples at a much lower temperature, 700°C, for an extended duration of 20 minutes. With enough carrier confinement in the QWs and with the proper annealing scheme, we obtain emission from metamorphically grown QWs as strong as, and sometimes even stronger than, that from similar single QW structures pseudomorphically grown on GaAs.
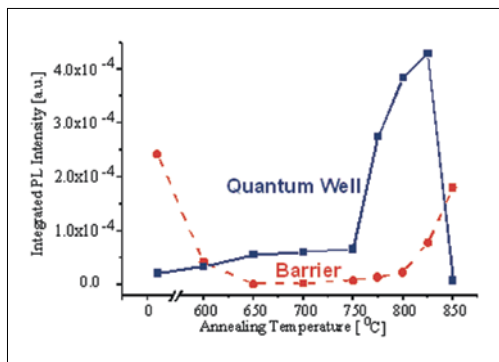
Figure 1: Integrated low temperature (19K) PL intensities from the QWs and the barriers as a function of the annealing temperature.
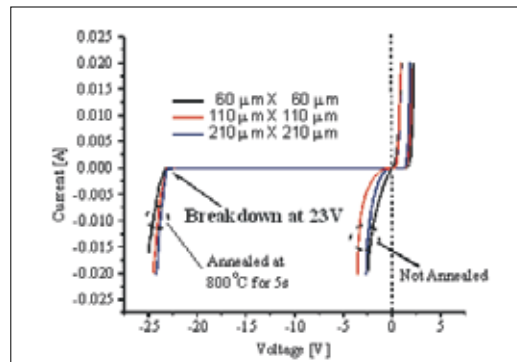
Figure 2: I-V characteristics of the diodes before and after 5 s rapid thermal annealing at 800 °C..

REFERENCES:

[1] Choy, H.K.H., "Quantum Wells on Indium Gallium Arsenide Compositionally Graded Buffers Realized by Molecular Beam Epitaxy," Ph.D. Thesis, EECS, MIT, January 2005

[2} Choy, H.K.H., C.G. Fonstad, Jr., "Enhanced Room Temperature PL from Metamorphic InGaAs/ InGaAlAs Quantum Wells on InGaAs Graded Buffers after Thermal Annealing," submitted for publication, in review.

Strain-Induced Photoluminescence Degradation in Metamorphically Grown InGaAs Quantum Wells

H.K.H. Choy, C.G. Fonstad, Jr
Sponsorship: Charles Stark Draper Laboratory, SMA, NSF

We have recently demonstrated that room-temperature PL of both tensilely and compressively strained quantum wells (QWs) grown metamorphically on graded buffers is strongly degraded relative to that of unstrained wells grown metamorphically on the same substrates [1]. For compressively strained QWs, it was found that the strain also brings about a strong temperature dependence of the PL. The integrated room-temperature and low temperature (19K) PL intensities are plotted against the indium compositions in the QWs in Figures 1 and 2, respectively. The degradation can be partially suppressed by reducing the grading rate of the buffer, by using a superlattice after the growth of the buffer, or by inserting a single 5-nm, tensile-strained GaAs layer and a 30-s growth interruption immediately before the growth of the QW. The PL can also be significantly improved if the substrate temperature during the growth of the graded buffers is reduced when the indium content in the graded buffer is high.

Our observations lead us to conclude that the degradation we observe, which has not been observed previously, is unrelated to the Matthews-Blakeslee process. We, instead, believe that the degradation is most likely related to the surface morphology introduced by the graded buffers, and that the surface roughness, which develops during growth of graded buffer layers plays the key role in the reduction. We also propose that one may eliminate the degradation by smoothing the linearly graded buffer layer using chemical-mechanical polishing (CMP) prior to growing a metamorphic QW structure on it. Such a sequence, if successful, offers another pathway to producing long-wavelength opto-electronic devices on GaAs substrates.
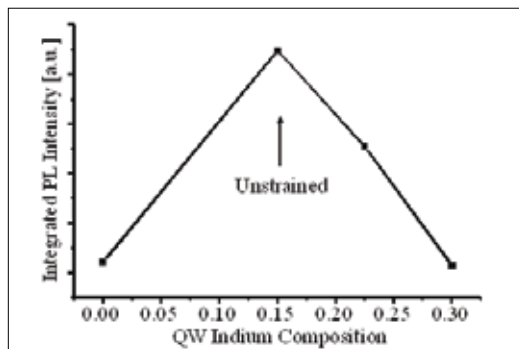
Figure 1: The integrated room temperature-PL intensities plotted against the indium compositions in the QWs.
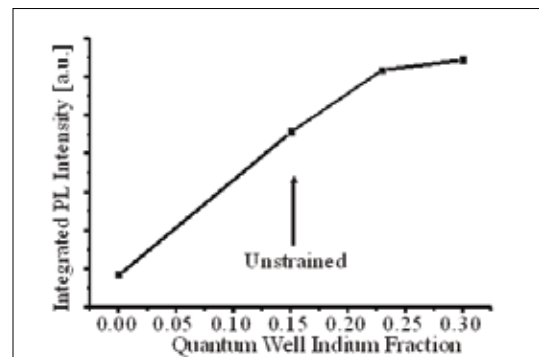
Figure 2: The integrated low temperature (19K) PL intensities of the same set of samples as in Figure 1.

REFERENCES:

[1]   Choy, H.K.H., "Quantum Wells on Indium Gallium Arsenide Compositionally Graded Buffers Realized by Molecular-beam Epitaxy," Ph.D Thesis, EECS, MIT, Cambridge (MA): 2005. See also by same authors: "Strain-induced Photoluminescence Degradation of InGaAs/ InGaAlAs Quantum Wells Grown Metamorphically on InGaAs Graded Buffers," submitted for publication, in review.

Monolithic Integration of InAlGaP-based Yellow-green Light Sources on Silicon

M.J. Mori, J.W. Wu, L. McGill, E.A. Fitzgerald

Unlike those of the III-Nitrides, the lattice parameters of the InAlGaP system are amenable to integration on silicon. The wide, direct bandgap of InAlGaP makes the material an excellent candidate for green-light emission, for which the human eye is the most sensitive. We are working to optimize and integrate yellow-green-emitting devices monolithically on silicon via compositionally graded buffers. With integration, high-efficiency micro-displays with lithographically defined pixels as well as CMOS-driver electronics are possible. Additionally, since absorption length is a strong function of photon energy in silicon, yellow-green wavelengths (where $\alpha_{Si} \sim 10^4\,\text{cm}^{-1}$) are optimal for high-speed, low-cost Si photodetectors. With a bright light source, this visible wavelength may be the best choice for chip-to-chip optical interconnects. Our current work focuses on InAlGaP materials with lattice parameters near that of GaAs and we have already demonstrated a yellow-green epitaxial-transparent-substrate light-emitting diode (LED) in [1]. These LEDs will be directly ported to silicon substrates with our optimized, compositionally graded buffer technologies (such as InGaP/GaP or SiGe/Si), which enable high-quality lattice-mismatched epitaxy of InAlGaP. The LEDs consist of an undoped, compressively strained quantum well (QW) grown on an $In_{0.22}(Al_{0.2}Ga_{0.8})_{0.78}P/\nabla_x[In_x(Al_{0.2}Ga_{0.8})_{1-x}P]/$GaP virtual substrate. Theoretical modeling of the structure predicts an accessible wavelength range of approximately 540nm to 590nm (green to amber). Peak emission at 570nm was observed by cathodoluminescence studies of undoped structures with a QW composition of $In_{0.35}Ga_{0.65}P$. The QW-LEDs emit with a primary peak at 590nm and a secondary peak at 560nm. The highest LED power of 0.18μW per facet at 20mA was observed for a QW composition of $In_{0.32}Ga_{0.68}P$ and a bulk threading dislocation density on the order of $7 \times 10^6\,\text{cm}^{-2}$. Based upon superspots present in electron diffraction from the quantum well region, we believe that the observed spectrum is the result of emission from ordered and disordered domains in the active region.
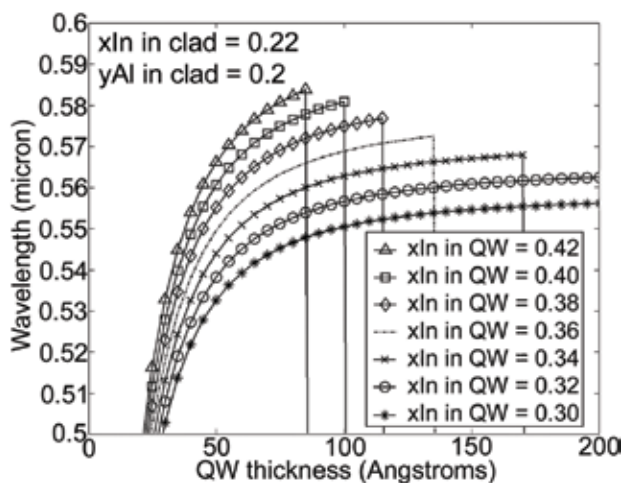
Figure 1: Predicted emission for subcritical-thickness quantum-well devices with $In_{0.22}(Al_{0.2}Ga_{0.8})_{0.78}P$ cladding and an $In_xGa_{1-x}P$ strained quantum well. Vertical lines represent the critical-thickness cutoff.
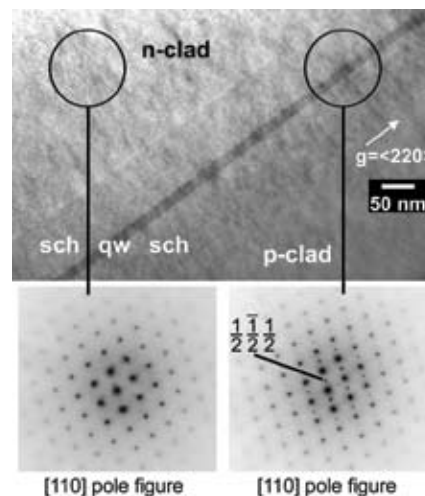
Figure 2: Cross-section transmission electron micrograph of a device with an $In_{0.32}Ga_{0.68}P$ quantum well. Electron diffraction of the quantum well shows ordering superspots, while the clad does not.

REFERENCES:

[1]   McGill, L., J. W. Wu, E.A. Fitzgerald, "Yellow-green Strained-InGaP Quantum-well Epitaxial-transparent-substrate Light-emitting Diodes," *Journal of Applied Physics*, vol. 95, pp. 7561-7566, June 2004.

Mid-10^5 cm^{-2} Threading Dislocation Density in Optimized High-Ge Content Relaxed Graded SiGe for III-V Integration with Si

D.M. Isaacson, A.J. Pitera, C.L. Dohrman, S. Gupta, E.A. Fitzgerald
Sponsorship: MARCO MSD

The relaxed graded SiGe platform ($\nabla_x[Si_{1-x}Ge_x]/Si$) has been enormously successful for fabricating high-mobility strained-Si and strained-Ge devices, as well as for the Ge/$\nabla_x[Si_{1-x}Ge_x]$/Si platform for the subsequent growth of III-V devices, such as: lasers, waveguides, and high-efficiency solar cells. The key feature of the relaxed graded SiGe buffer approach is its effectiveness at minimizing threading dislocation densities, thereby allowing for fabrication of scaleable Ge/$\nabla_x[Si_{1-x}Ge_x]$/Si structures with TDD values on the order of 10^6 cm^{-2}.

Despite these successes, two key factors have room for improvement with respect to III-V integration on SiGe buffer: a further reduction in the threading dislocation density as well as a reduction in the high thermal mismatch portion of the SiGe buffer. This work presents a framework for achieving these goals. By avoiding dislocation nucleation in $Si_{1-x}Ge_x$ layers of x>0.96, we have achieved a relaxed $Si_{0.04}Ge_{0.96}$ platform on Si(001) offcut 2° that has a threading dislocation density of 7.4×10^5 cm^{-2}, with no fundamental limitation to obtaining lower values. This 2° offcut orientation was determined to be the minimum necessary for growth of GaAs without anti-phase boundaries (APBs). Furthermore, we found that we could compositionally grade the Ge content in the high-Ge portion of the buffer at up to 17%Ge µm^{-1} with no penalty to the threading dislocation density. The reduction in both threading dislocation density and buffer thickness exhibited by our method is an especially significant development for relatively thick III-V based minority-carrier devices, such as multi-junction solar cells and vertical cavity surface emitting lasers.
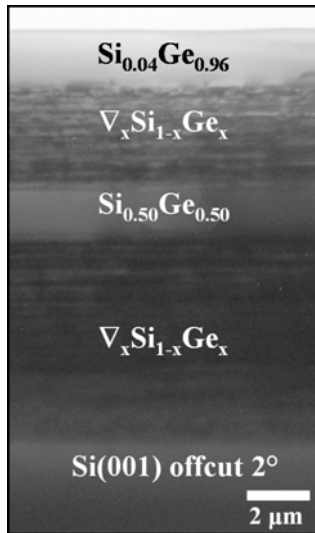
Figure 1: Cross-sectional transmission electron microscopy image of the optimized $Si_{0.04}Ge_{0.96}$/$\nabla_x[Si_{1-x}Ge_x]$/Si platform.
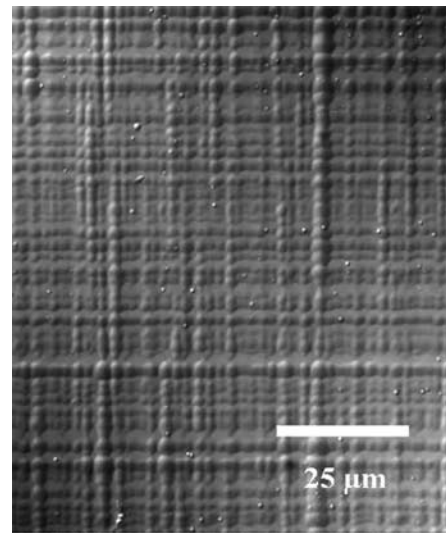
Figure 2: Nomarski etch-pit density image of the optimized $Si_{0.04}Ge_{0.96}$/$\nabla_x[Si_{1-x}Ge_x]$/Si platform.

A Bonding Apparatus for OptoPill Assembly

M.S. Teo, C.G. Fonstad, Jr.
Sponsorship: MARCO IFC, NSF

The central objective of our heterogeneous integration effort is to integrate III-V functionality, such as laser emission, with Si-CMOS circuitry in a manner that retains all of the advantages of multi-wafer, batch processing that have propelled Si ICs along the Moore's Law performance timeline for so long. To this end, we have developed Recess Mounting with Monolithic Integration, RM^3, in which we place III-V heterostructure pills, or OptoPills, in recesses 5 to 6 microns deep and 50 microns in diameter that are formed in the inter-metal dielectric layers covering a processed Si IC, and then interconnect them monolithically with the underlying circuitry.

Once the hetero-structure device pills have been placed in their recesses, whether using micro-scale pick-and-place or fluidic self-assembly (both described in other abstracts), they must be securely fastened in place. Making a good electrical contact to the bottom of the pill is often desired at the same time. Two different solders have been found particularly suitable for this purpose: a Au-Sn eutectic to solder gold-coated pills into the recesses and a Pd-Sn-Pd stack to bond bare pills into the recesses. In both cases it is necessary to supply pressure between the pill and substrate to reliably achieve successful bonding or soldering. To apply the required pressure to these micro-scale pills, particularly when they are in recesses, we have developed a bonding system, shown in Figure 1, in which a vacuum-bagging film and a pressure differential are used to apply a controlled, reproducible, and uniform pressure simultaneously to all the pills on a wafer. A photograph of the unit, with the outer chamber removed so the film is visible, appears in Figure 2. Typical bonding conditions apply a pressure of approximately 50 psi and a temperature of approximately 300°C.
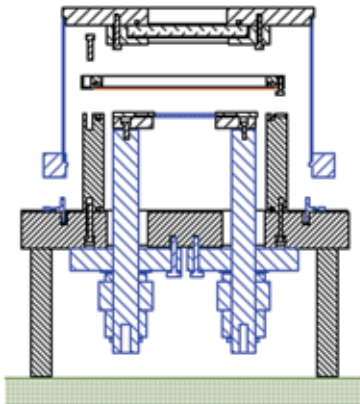
Figure 1: Cross-sectional drawing of the bonding chamber showing the base plate with heater strip, the inner bonding-ambient chamber, the film holder plate, and the outer pressurized chamber.
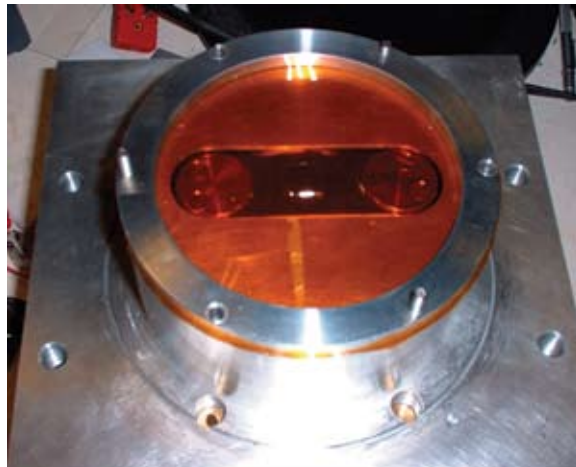
Figure 2: The film-pressure bonding system shown with the outer, pressurized chamber removed to show the film and heater strip.

REFERENCES:

[1]   Teo, M.S., "Development of Pick-and-Place Techniques for Monolithic OptoPill Integration," S.M. Thesis, Department of Electrical Engineering and Computer Science, MIT, January, 2005, unpublished.

Micro-scale Pick-and-Place Integration of III-V Devices on Silicon

M.S. Teo, D. Chang, C.G. Fonstad, Jr.
Sponsorship: MARCO IFC, NSF

We are developing micro-scale assembly techniques for integrating III-V optoelectronic devices on silicon integrated circuits that blur the practical distinction between hybrid and monolithic integration. Our general approach, which we term Recess Mounting with Monolithic Integration, or RM^3, involves forming recesses 5 to 6 microns deep and 50 microns in diameter in the inter-metal dielectric layers covering a processed Si IC. After all of the standard silicon processing is completed, the Si IC wafers for RM^3 integration undergo further back-end processing, first to create the recesses, and then to place and bond III-V device structures in them. Wafer-level processing is continued to complete any remaining III-V device processing and to interconnect those devices with the underlying electronic circuitry. One approach we have taken to placing the III-V devices in recesses has been to form discrete heterostructure pills the size of the recesses, and to place them individually into the recesses using micro-scale pick-and-place assembly, as illustrated in Figure 1.

The dimensions of the device pills we are assembling are much smaller than the device die normally used in pick-and-place applications, and thus conventionally available vacuum pick-up tools are unsuitable. We have found, however, that quartz micropipettes of the type used by microbiologists to study cells can be fabricated with the right dimensions and geometry for this application. In particular, we use micropipettes pulled from 1-mm-diameter, 0.25-mm-wall quartz tubing and tapered down over 7 mm to a tip diameter of 30 microns. The tip is beveled at 45° to complete the pick-up tool. A photomicrograph of a tool mounted in its holder is shown in Figure 2. With this tool, pills can be picked up, placed in a recess, and released without damage [1].

Our current effort is directed at using micro-scale pick-and-place assembly to do heterogeneous integration and further developing and refining the technique.
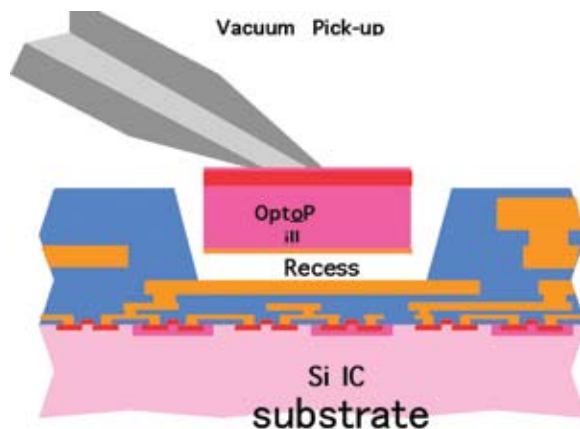
Figure 1: A cartoon illustrating the micro-scale pick-and-place process for locating a heterostructure device pill in a recess on a Si IC wafer surface.

Figure 2: A quartz micropipette pick-up tool mounted on its holder.

REFERENCES:

[1] Teo, M.S. "Development of Pick-and-Place Techniques for Monolithic OptoPill Integration," S.M. Thesis, Department of Electrical Engineering and Computer Science, MIT, January 2005, unpublished.

Magnetically Assisted Statistical Assembly of III-V Devices on CMOS

J. Rumpler, J.M. Perkins, C.G. Fonstad, Jr.
Sponsorship: SRC, MARCO IFC, NSF, SMA

We are researching an efficient process for integrating III-V devices on silicon CMOS using fluidic self-assembly and a unique magnetic retention mechanism. Specifically, III-V devices and silicon ICs will first be processed separately. Dielectric recesses 5 to 6 microns deep and 50 to 60 microns in diameter will then be formed on the IC wafer surface, and permanent ferromagnetic films will be deposited and patterned at the bottoms of these recesses. The III-V devices will be etched into similarly sized pillars that will then be embedded in a polymer, and the substrate will be removed. A permeable ferromagnetic film will next be patterned on the back side of the devices, and they will be released from the polymer. The resulting pills will be cascaded over the CMOS wafer in a fluid, where they will fall into the recesses and be retained by short-range magnetic forces. They will finally be bonded in place and interconnected with the underlying electronic circuitry, using techniques developed in our earlier integration research.

We have demonstrated experimentally that the proposed magnetic retention works and that pills formed, as just described are attracted to and held by patterned magnetized films [1]. We have also conducted fluidic assembly experiments in which thousands of 45 μ diameter, 6 micron thick III-V pills are flowed over a target substrate containing hundreds of correspondingly sized dielectric recesses in the apparatus shown in Figure 1. Initial fluidic assembly experiments without magnetic retention show that a large number of pills can be successfully assembled, as shown in Figure 2, but it is also found that the pills readily come out of the recesses when, for example, the substrate is removed from the fluid. This clearly demonstrates that a short-range retention force is essential to a practical self-assembly process, and in the near future, we hope to demonstrate high yield assembly and retention using magnetic attraction.
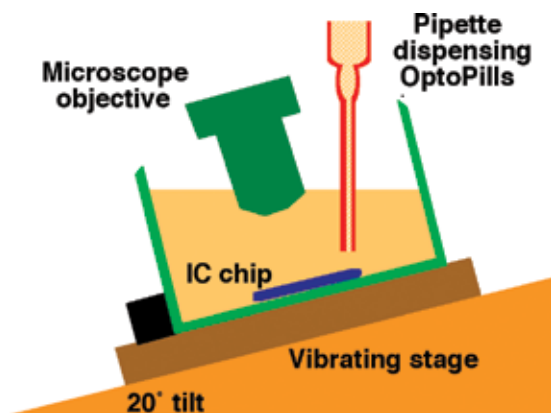
Figure 1: Assembly setup.
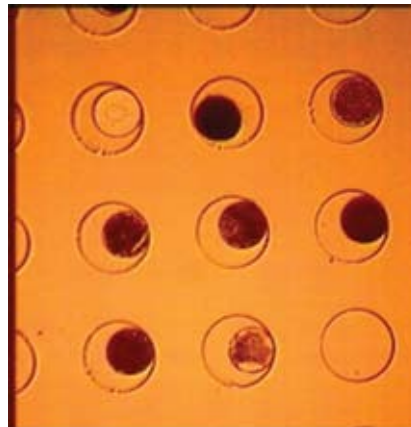
Figure 2: An array of silicon dioxide recesses filled by GaAs devices.

REFERENCES:

[1]   Rumper, J.J., J.A. Perkins, C.G. Fonstad, Jr., "Use of Patterned Magnetic Films to Retain Devices During Fluidic Self-Assembly," to be submitted for publication.

Integration of 1.5-µm P-i-N Diodes on Si ICs for Optical Clocking and Interconnects

Y.-S. V. Lei, C.G. Fonstad, Jr. in collaboration with D. Boning
Sponsorship: MARCO IFC

An important issue faced by designers of high performance microprocessors is distributing the clocking signals uniformly across an integrated circuit chip. While transistor dimensions are successfully being aggressively scaled down to meet the insatiable demand for higher processor speeds, the accompanying shrinkage of metal interconnect dimensions has led to increased signal propagation delays, and to severe clock distribution problems. Distributing clock signals optically, rather than electrically, may offer a solution to this problem because doing so eliminates many of the problems associated with electrical interconnect lines. To explore this option, we are applying our optoelectronic integration techniques to integrate of III-V semiconductor P-i-N photodiodes on a variation-robust Si-CMOS optical clock receiver circuit (which is shown in Figure 1) that has been designed by Prof. Boning and his group at MIT. The integration technique employed is referred to as recess-mounting with monolithic metallization, or RM[3]

integration for short. The integration process involves several major steps: a) recess formation, b) assembly and bonding of the photonic device heterostructures [1], c) ohmic contact formation, d) device active area definition, e) planarization and passivation, f) via opening, and g) top metallization [2].

Our recent focus has been on the fourth step in this sequence, in particular on refinement of the dry etching technique process for defining the photodiode active region. A process employing BCl_3/He chemistry has shown particularly promising results. The next step will be to fabricate discrete InGaAs/InP photodiodes in order to study and characterize their electrical and optical behaviors independently from the Si-CMOS circuits. Then we will use the processes and technology we have developed to integrated similar photodiodes on the Si-CMOS circuit chip shown in Figure 1.
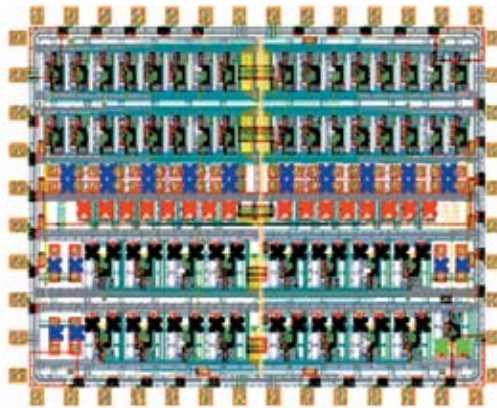
Figure 1: The layout of a Si-CMOS optical clock distribution chip designed by Professor Boning's group at MIT. The 60-x 60-µm recesses (marked with "X"s) are areas where the photo-diode will be placed. The die is 2.7mm x 2.1mm.

REFERENCES:

[1] Teo, M.S., "Development of Pick-and-Place Techniques for Monolithic OptoPill Integration," S.M. Thesis, Department of Electrical Engineering and Computer Science, MIT, January, 2005, unpublished.

[2] Lei, Y.V., "Post-Assembly-Process Development for Monolithic OptoPill Integration on Silicon CMOS" Ph.D. Thesis, EECS, MIT, June 2004.

Integration of III-V In-Plane SOAs and Laser Diodes with Dielectric Waveguides on Silicon

E.R. Barkley, J.J. Rumpler, S. Famini, C.G. Fonstad, Jr.
Sponsorship: DARPA through ARL

The successful implementation of optical interconnects on silicon requires the ability both to integrate III-V optoelectronic devices on silicon substrates with dielectric waveguides and to achieve low-loss optical coupling between the devices and the waveguides. Building on the success of ongoing research in recessed mounting with monolithic metallization (RM^3) of III-V device pills on silicon [1], this project ultimately seeks to demonstrate optical amplification of an on-chip signal through an RM^3 integrated InP/InGaAsP semiconductor optical amplifiers (SOA) and low-loss end-fire coupling from an integrated, edge-emitting laser diode to a dielectric waveguide. A schematic of a III-V SOA integrated with a silicon oxynitride waveguide is shown in Figure 1.

At this stage of the project, the focus falls on developing a process and design that enable low loss coupling between the waveguide and the III-V device. Achieving low loss coupling requires careful processing to ensure smooth sidewalls and facets and attention to the optical mode characteristics of the waveguiding components. Silicon oxynitride waveguides have been fabricated and are currently undergoing testing; Figure 2 shows a cross-sectional SEM photograph of a representative guide. Finite difference time domain (FDTD) simulations have been run to quantify the anticipated coupling loss as a function of the waveguide-to-SOA separation. Based on previous device placement and mounting results, an estimated 2-μm separation is achievable, corresponding to a 4dB/facet loss, as obtained from FDTD simulations.

As a supplement to the ongoing RM^3 research, a micro-cleave technique is being explored as a way of obtaining cleaved facets on small (100 μm x 50 μm) III-V devices. This technique will enable laser length definition with micron-level precision. Future work will involve exploring additional ways of decreasing the waveguide to device coupling losses using, for example, anti-reflection coated devices and tapered waveguides.
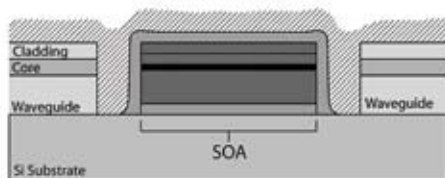
Figure 1: Schematic of an SOA integrated with a dielectric waveguide.
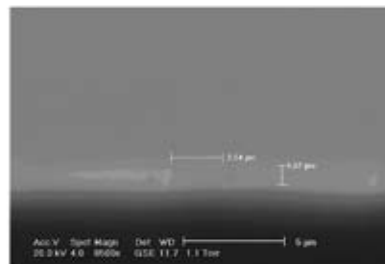
Figure 2: SEM of the waveguide cross-section.

REFERENCES:

[1] See companion abstracts in this document for more information on the RM^3 integration process: A) "Microscale Pick-and-Place Integration of III-V Devices on Silicon" Teo, Chang, Fonstad. B) "Magnetically Assisted Statistical Assembly of III-V Devices on CMOS," Rumpler, Perkins, Fonstad

Integration of VCSELs on Si ICs for Free-Space Optical Neural Network Signal Processing

J.M. Perkins, C.G. Fonstad, Jr., in collaboration with T. Simpkins, C. Warde
Sponsorship: NSF, SRC

This research aims to integrate AlGaAs vertical-cavity, surface-emitting lasers (VCSELs) onto silicon integrated circuits, using integration techniques developed and refined by Professor Fonstad's group. In these techniques, such as Micro-scale Pick-and-Place (MPAP) and Magnetically Assisted Statistical Assembly (MASA) [1], device pills are bonded in recesses on a silicon wafer surface and connected monolithically to the underlying silicon circuitry. In this study the pills will be small cylindrical III-V disks around 75 microns in diameter and 7 microns in height. Each pill will contain one partially processed VCSELs fabricated on campus from a commercially grown AlGaAs epi-wafer. The necessary heterostructure design has been completed and the epi-wafers have been ordered. A processes flow for the fabrication of the VCSEL devices has also been designed and is currently under development. The structure will utilize an oxide current-confinement layer. Once the mask design has been finalized for the semiconductor etching and the metallization steps, the processing of VCSEL

devices will begin. These devices will first be measured on their native substrate to test their basic functionality. The VCSEL devices can then be freed from their substrate and bonded onto a Si IC substrate. New technology must be developed to release pills with an InGaP etch-stop layer, and to deposit and pattern metal on the backs of the released pills.

The specific application this work pursues is a free-space, optical neural network array signal processor [2], which will use a 3x3 array of VCSELs in each pixel, shown in Figure 1, and holographic elements between pixel planes, shown in Figure 2, to allow communication between each pixel in one array, to any of nine different pixels in the following pixel array. For this reason, the VCSELs in this study will emit at 850nm, a wavelength compatible with silicon detectors. Professor Cardinal Warde and his MIT students are responsible for the array and optics parts of the effort.
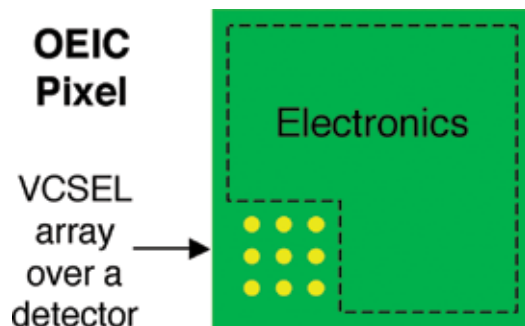
Figure 1: A schematic illustration of a typical pixel in the arrays on each level of the free-space, optical neura network array signal processor under development. The 3x3 VCSEL array will allow communication to any of nine pixels in the next level of the multi-level system.
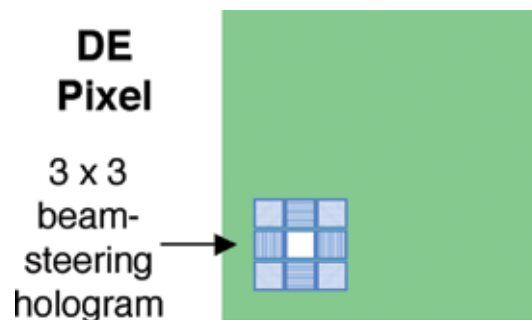
Figure 2: A schematic illustration of a typical pixel in the dielectric element arrays between the OEIC pixel arrays described in Figure 1. The beam-steering hologram directs the output of each of the nine VCSELs in a pixel to the detectors associated with each of nine different pixels on the next plane of OEIC pixels.

REFERENCES:

[1]   Fonstad, C.G. Jr., "Magnetically Assisted Statistical Assembly - A New Heterogeneous Integration Technique," Singapore-MIT Alliance Symposium, Jan 2002, unpublished; M. S. Teo. "'Development of Pick-and-Place Assembly Techniques for Monolithic OptoPill Integration," S. M. Thesis, MIT Department of Electrical Engineering and Computer Science. January 2005, unpublished.

[2]   Warde, C, C.G. Fonstad, Jr., "Compact Optoelectronic Neural Co-processor Project," in Proceedings of the International Conference on Opto-electronics and Laser Applications, ICOLA '02, October 2-3, 2002, Jakarta, Indonesia, pp. B07-B11.

Germanium Photodetectors for Silicon Microphotonics

J. Liu, D. Ahn, D.T. Danielson, D. Pan, W. Giziewicz, C.-Y. Hong, K. Wada, J. Michel, L.C. Kimerling
Sponsorship: Pirelli Lab, S.P.A., Analog Devices

Silicon microphotonics is emerging as a promising technology for optical communications and on-chip interconnects. One of the critical devices required is a high-performance photodetector compatible with standard silicon complimentary metal-oxide-semiconductor (CMOS) technology. We have demonstrated an epitaxial Ge photodetector on Si as a promising candidate in previous reports. Here we report a higher-performance and broader spectrum Ge photodetector by utilizing tensile strain introduced by the thermal annealing process.

Smooth Ge epitaxial layers with a root-mean-square roughness of ~0.7 nm were selectively grown directly on Si in windows opened through a SiO_2 layer. Due to the thermal expansion mismatch between the Ge epitaxial layer and the Si substrate, 0.20% in-plane tensile strain was introduced into the Ge layer, reducing the direct band-gap of Ge from 0.801 to 0.773 eV and extending the effective photodetection range to 1605 nm. The tensile strain can be further enhanced by the backside silicidation process. The device shows a high responsivity over a broad detection spectrum from 650 to 1605 nm (Figure 1), and a 3 dB bandwidth of 8.5 GHz at a low reverse bias of 1 V (Figure 2), having promising applications in both telecommunications and integrated optical interconnects.

One other important component in optical circuitry is the integration of photodetectors and waveguides. Integration benefits detector performance by circumventing the usual trade-off problem between responsivity and bandwidth. In contrast to the more common III-V materials case in which both waveguide and photodetector are lattice-matched semiconductor materials and are grown in one-step epitaxial process, we adopted SiON/Si_3N_4 dielectric materials for waveguides and group IV Si/Ge materials for photodetectors, for monolithic integration with a Si CMOS chip. This design requires a novel coupling structure. We have investigated coupling behavior for Group IV integrated photodetectors. We fabricated a photodetector mesa structure with enough cladding height to optically isolate the waveguide from substrate. We employed a CMP planarization step to form a platform on which the waveguide can be deposited. To achieve efficient and uniform optical coupling between waveguide and photodetectors, the effects of design variations are measured and compared with theoretical studies based on analytic modeling and BPM (Beam Propagation Method) optical simulation.

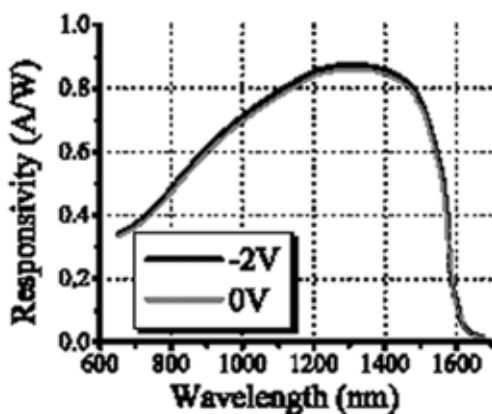Figure 1: The DC responsivity at 0V and 2V reverse bias in the wavelength range of 650-1650nm without antireflection coating.

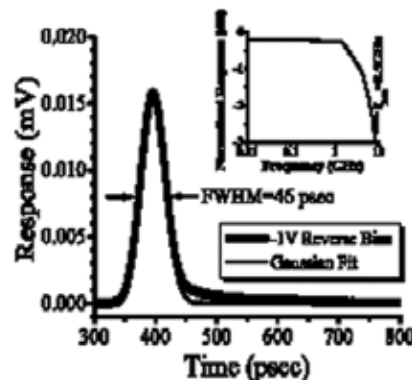Figure 2: Temporal response of a 10×70µm Ge/Si photodetecter at a reverse bias of 1V to ~1 ps-long pulses generated by a mode-locked Yb-fiber laser at 1040 nm (black line). The inset of the figure shows the Fourier transform of the pulse, which gives a 3 dB bandwidth of 8.5GHz.

Quantum Dot Photodetectors

A.C. Arango, D.C. Oertel, M.G. Bawendi, V. Bulovic
Sponsorship: MIT ISN

Solution-processable colloidal quantum-dot systems exhibit many of the special optical and electronic properties associated with epitaxially grown, quantum confined systems. Their tunable band gap and higher absorption relative to the bulk make quantum dots particularly attractive as photo-generation materials. At the same time, colloidal quantum dots offer much greater material system flexibility than epitaxial quantum dots because deposition on any substrate is possible.

Efficient photoconductivity has previously been observed in lateral device structures consisting of single thin quantum dot films [1]. Response time of this device was limited by charge transport, suggesting that a vertical photodetector structure could decrease the response time and support higher currents due to the larger contact cross-sections. That motivates our present project, in which we study the photo-response of quantum dot thin films in a vertical sandwich structure. We engineer a multilayer thin film device with a colloidal quantum dot film inserted into the middle of a wide bandgap structure forming a double heterojunction device that functions as a rectified diode (Figure 1). The rectifying behavior ensures suppression of the shunt current in the reverse-biased structure that can arise from the mechanical imperfections in the quantum dot film. Additionally, the photo-generative quantum dot film can be positioned in the peak of the optical field, increasing the device efficacy. Changing the size and material properties of the quantum dots tunes the response spectrum of the device across visible and near infra-red spectra.

With current-voltage measurements (not shown), we have achieved low dark current and have identified high internal resistance of the cadmiun selenide (CdSe) quantum-dot film as a major limitation to the device performance. The quantum efficiency (number of generated electrons per incident photon) is shown in Figure 2. At present we focus on improving the device performance and optimizing the photodetection response in the 1um-to-2um wavelength region by using lead selenide quantum-dot films.
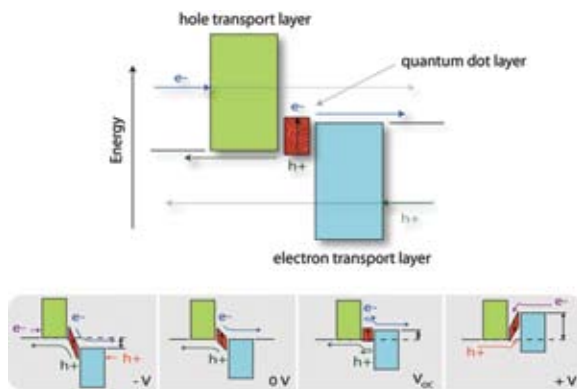
Figure 1: Alignment of energy bands in a conceptual tri-layered p-i-n-like quantum dot hetero-junction photo-detector. The contact layers (indicated in green and blue) serve to transport charge out of the device, block charge from entering the device, and transmit light to the absorbing quantum dot layer. Under applied bias, the proposed device exhibits rectification because charge is blocked at both electrodes under reverse bias yet allowed to enter under forward bias.
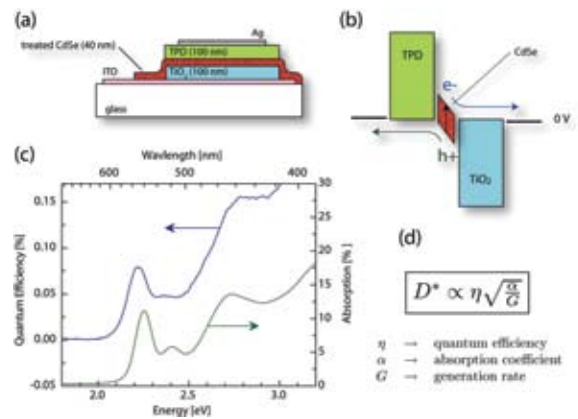
Figure 2: The photo-detector device structure (a) consists of a solution-deposited, colloidal CdSe, quantum-dot layer sandwiched between n-type TiO_2 and a p-type organic semiconductor TPD. At zero bias and under illumination (b), an excited electron can exit the device via the TiO_2 layer, while the corresponding hole can exit via the TPD. The resulting quantum efficiency spectrum at zero bias (c) tracks the shape of the CdSe absorption. An important metric for photo-detectors (especially infrared detectors) is the detectivity D* (d), a measure of a device sensitivity to background noise.

REFERENCES:

[1]   Jarosz, M.V., V.J. Porter, B.R. Fisher, M.A. Kastner, and M.G. Bawendi, "Photoconductivity Studies of Treated CdSe Quantum Dot Films Exhibiting Increased Exciton Ionization Efficiency," *Phys. Rev. B*, vol. 70, no. 19, art. 195327, November 2004.

Integrated Emitter/Detector/Electronics Arrays for Diffuse Optical Tomography

C.G. Fonstad, Jr., W.P. Giziewicz, in collaboration with C. Saunders, D. Brooks, S. Prasad, R. Gagnon (Northeastern University)
Sponsorship: NSF

Biomedical imaging and sensing may benefit greatly from development of integrated probes because they promise improvements in signal-to-noise ratio, as well as, reduced size and cost. We are working to apply the optoelectronic integration technologies we are developing to create an integrated circuit implementation of a probe for diffuse optical tomography (DOT), in which emitters, detectors, and driver, receiver, and signal-processing circuitry, fabricated in a standard analog CMOS process, are integrated together on a single chip.

The first lot of DOT chips was received from MOSIS in late 2003. Testing indicated that the stand-alone detectors functioned well and as anticipated. Specifically, Gagnon and Giziewicz show that the detectors have the high sensitivity at low light levels, large dynamic range, and low dark currents needed for the targeted DOT applications [1]. The associated detector circuitry, however, did not function properly. Extensive testing led ultimately to the discovery of several layout errors and circuitry errors. These were corrected and another chip design, including most of the original components as well as additional cells and circuitry, was prepared by Giziewicz and submitted to MOSIS in early 2004. Chips were received in June 2004.

Northeastern University S.M. student Christopher Saunders is completing the characterization and testing of the latest chip, and will perform simulated DOT sensing with the chip using external fiber sources. Simultaneously, work is proceeding in another program on the integration of VCSELs on Si CMOS chips; if that work proceeds as planned, emitters will be integrated on the DOT chip as well, and Saunders will test the fully integrated DOT chips before he completes his S.M. thesis research (and the NEU program terminates) at the end of August 2005.
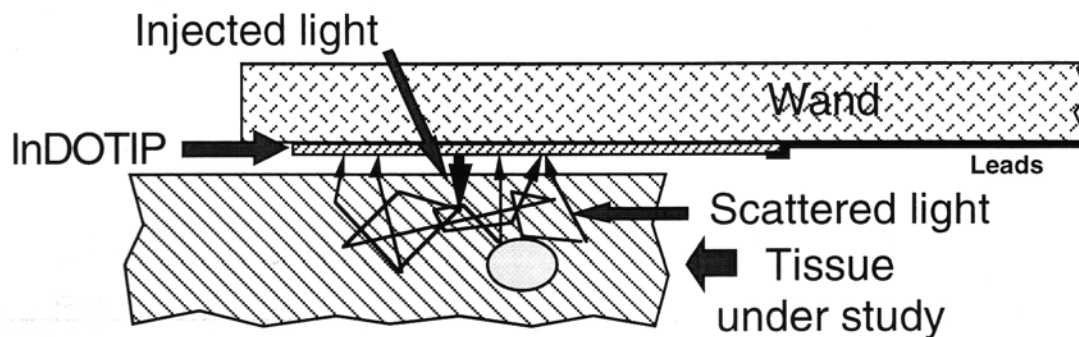
Figure 1: An illustration of one way that the DOT OEIC die might be mounted on the end of a wand and used for DOT subsurface imaging of soft body tissue. In use, each VCSEL is illuminated in turn (the figure shows one turned on) and the pattern of scattered light seen by the detector array is recorded. With this information, an image of the sub-surface structure can be constructed.

REFERENCES:

[1]   Giziewicz, W.P., R. Gagnon, S. Prasad, D. Brooks, C.G. Fonstad, Jr., "Initial Development of an Integrated Optoelectronic Probe for Biomedical Imaging," Proceedings of the 26th Annual International Conference of the IEEE Engineering in Medicine and Biology Society, EMBC 2004, San Francisco, CA, Vol.3, pp. 2094-2097, 2004.

Fabrication of Superconducting Nanowire, Single-Photon Detectors

J.K.W. Yang, R. Hadfield, G. Gol'tsman, B. Voronov, K.K. Berggren
Sponsorship: MIT Lincoln Laboratory

Several novel applications that rely on high-speed single-photon detectors (SPDs), for example quantum cryptography, have recently emerged. The nanowire SPD consists of a 4-nm-thick, ~ 100-nm-wide, superconducting NbN wire operating at 4.2 K or below. It reportedly detects single photons at 1550-nm wavelength with a detection efficiency (DE) of ~ 5%, which is too low to be of use for most applications. Its proposed GHz-counting rate is several orders of magnitudes faster than has been demonstrated by other types of SPDs to date [1]. The aim of our research is to improve the detection efficiency (DE) of the nanowire SPDs and to make devices capable of GHz-counting rates. Figure 1 shows a scanning electron micrograph (SEM) of a nanowire SPD that consists of closely spaced nanowires in a large-area meander. We are working to improve DE by: (1) using thicker and more optically absorptive NbN films, (2)

defining even narrower nanowires, (3) improving the linewidth uniformity, (4) increasing the length of the nanowire (and thus the total area of the meander), and (5) identifying and minimizing sources of material damage (such as electro-static discharge, plasma-damage, and thermal damage). We have recently developed a fabrication process using electron-beam lithography and hydrogen-silsesquioxane (HSQ) resist followed by a reactive-ion etch (RIE). This process, combined with an electron-beam proximity-effect correction technique, allows us to fabricate wires 150-μm long and less than 100-nanometer wide with line-width non-uniformity of ~ 5%, covering an area of ~ 25 μm^2 [2]. Figure 2 shows an SEM image of one of the devices we have made using this process that was 25-nm-wide: the narrowest superconducting nanowire ever fabricated for this type of detector.
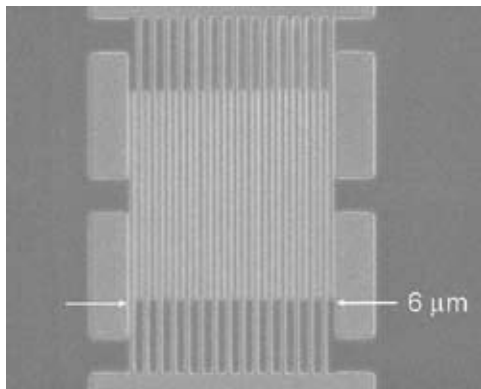
Figure 1:   SEM image showing a superconducting nanowire meander structure with uniform 100-nm-wide linewidths, fabricated using electron-beam lithography.
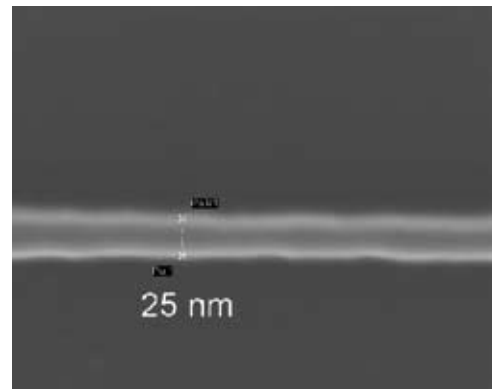
Figure 2:   SEM image of the narrowest superconducting wire that we have fabricated. Narrower wires will have higher detection efficiencies.

REFERENCES:

[1]   Verevkin, A., A. Pearlman, W. Slysz, J. Zhang, M. Currie, A. Korneev, G. Chulkova, O. Okunev, P. Kouminov, K. Smirnov, B. Voronov, G.N. Gol'tsman, and R. Sobolewski, "Ultrafast Superconducting Single-photon Detectors for Infrared-wavelength Quantum Communications," *Journal of Modern Optics*, v 51, n 9-10, 15 Jun-10 Jul 2004, pp. 1447-58, 2004.

[2]   Yang, J.K.W., E. Dauler, A. Ferri, A. Pearlman, A. Verevkin, G. Gol'tsman, B. Voronov, R. Sobolewski, W.E. Keicher, and K.K. Berggren, "Fabrication Development for Nanowire GHz-counting-rate, Single-photon Detectors," to be published in *IEEE Transactions on Applied Superconductivity*, 2005.

CMOS-compatible Photodetectors Using Ge-on-Si Films Deposited in an Applied Materials Epitaxial Reactor

O.O. Olubuyide, D.T. Danielson, L.C. Kimerling, J.L. Hoyt, in collaboration with J. Yasaitis (Analog Devices)
Sponsorship: DARPA, Analog Devices, Inc., IBM/SRC Graduate Student Fellowship

Germanium films have the required responsivity and speed to serve as photodetectors at the 1.55 micron range. Such detectors can be used in the communications field in a variety of high-speed systems, such as optical samplers. Thus, integrating Ge films grown on silicon (Ge-on-Si) substrates into a CMOS-compatible process is an attractive goal for making arrays of on-chip detectors that can be used in a range of electronic and photonic integrated circuit applications. In this project, we explore the growth properties and material quality of Ge-on-Si deposited by Low Pressure Chemical Vapor Deposition (LPCVD) in an Applied Materials Epitaxial Reactor, and the optical and electrical properties of Ge-on-Si photodiodes.

It has already been demonstrated in Ultra High Vacuum Chemical Vapor Deposition (UHVCVD) systems that depositing a low temperature Ge layer (seed layer), followed by the deposition of a high temperature layer with subsequent annealing, can create a smooth, planar Ge film on a <100> silicon substrate with threading dislocation density on the order of 10^7 cm^{-2} [1]. We have adapted this two-step deposition process to an LPCVD system. The effect of growth pressure, temperature, and seed thickness on the material quality has been explored. An optimum Ge seed layer deposition process window of $335^{\circ}C \pm 15^{\circ}C$ and 30 T $\pm$ 10 T (Figure 1) is identified and the requirement of a seed layer thickness above 30 nm (Figure 2) is demonstrated. After annealing at $900^{\circ}C$ for 30 minutes, these Ge films have threading dislocation densities of ~2 x 10^7 cm^{-2}. Recently, photodiodes fabricated with these optimized Ge films have been measured to have a dark current of ~1 µA for 50 µm square diodes at − 1 volt bias and a responsivity of 400 mA/W at 1.55 µm.
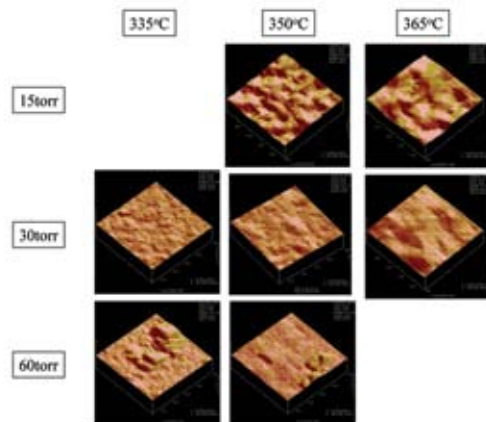
Figure 1: 1 µm x 1 µm AFM scans of Ge seed layers grown at various pressures and temperatures. As pressure increases, the growth rate increases, but gas phase nucleation (bottom panels) becomes an issue. At high temperatures, surface roughness increases due to the higher surface mobility of Ge. Optimum seed growth -conditions are $335^{\circ}C$ at 30 T.
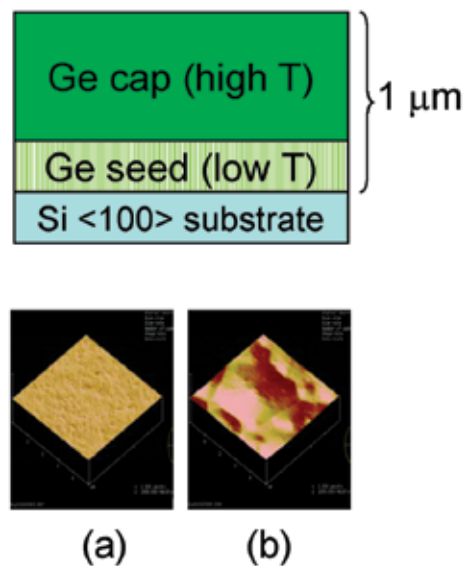
Figure 2: Ge film layer structure and 5 μm x 5 μm AFM scans of 1 μm-thick Ge films with different seed thicknesses: a) 60 nm seed, RMS of 0.9 nm and (b) 30 nm seed, RMS of 29 nm. The thicker 60 nm seed layer (a) has a higher thermal stability during the ramp to high temperatures for the thick Ge cap layer. and thus yields a significantly smoother surface morphology for the Ge film, in comparison to the thinner 30 nm seed layer (b).

REFERENCES

[1]   Luan, H.-C., D.R. Lim, K.K. Lee, K.M. Chen, J.G. Sandland, K. Wada, and L.C. Kimerling, "High-quality Ge Epilayers on Si with Low Threading-dislocation Densities," *Applied Physics Letters*, vol. 75, pp. 2909-2911, November 1999.

Chemo-sensing Optoelectronic Structures

J. Ho, A. Arango, T. Swager, V. Bulovic
Sponsorship: ISN, NSF-MRSEC

We are developing solid-state, organic device structures capable of efficiently converting analyte detection into an electrical signal. The main advantage to using organic materials is that they are synthetically flexible and can be tailored to respond in a distinct manner to specific analytes. Our proposed device structure is a heterostructure consisting of an optically active, chemo-sensing layer and a charge transport layer. Physically separating the sensing and transport functions in chemical sensors has two significant advantages. First, we can optimize both the sensing and the transport layers independently to maximize chemical sensitivity. Second, we can tailor materials in the sensing layer to detect specific materials, allowing us to reuse the same device structure for a variety of applications.

An integral part of this research is to demonstrate efficient, organic photo-transistors and to physically model their behavior.

By building upon models developed for organic transistors, we can begin to explain the behavior or organic photo-transistors. In the photo-transistor structure, light acts as a gate pseudo-electrode by changing the conductivity in the transistor channel to modulate current. Once the photo-transistor model has been developed and the material set has been optimized, the next challenge will be to introduce chemically sensitive materials into the structure of the device to modulate the photo-detection ability of the sensing layer. In this way, we can detect the presence of any analyte. By transducing the sensing response of an analyte into the transport of charge, we can observe a bulk change in the system with only a small number of binding events; thereby increasing the sensitivity of the devices.
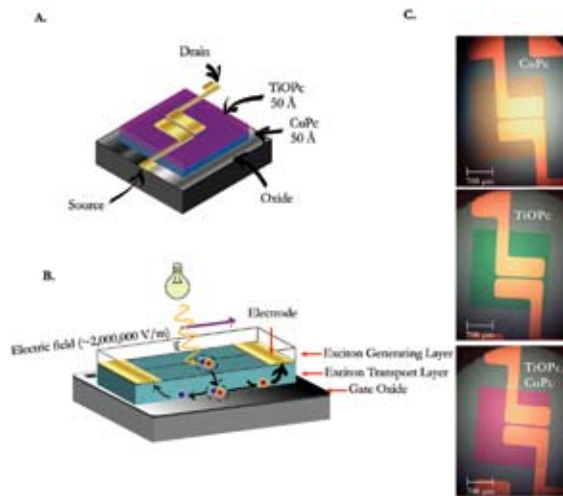
Figure 1: A) Schematic structure of a phototransistor. B) Schematic of phototransistor operation C) Microscope pictures of photoresistors under 40X magnification.
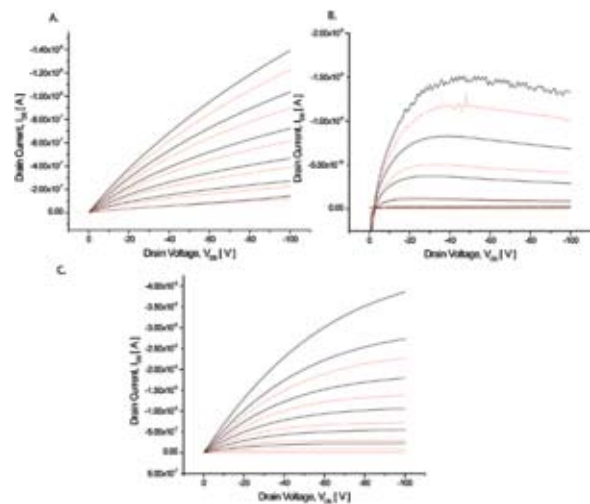
Figure 2: Linear I-V plots of A) 50 Å CuPc, B) 50 Å TiOPc, C) 50 Å CuPc, and 50 Å TiOPc. The dotted red lines represent I-V curves in the absence of light for gate voltages ranging from 0 V to -100 V in steps of -20 V. The dashed black lines represent the same curves In the presence of white illumination. Notice that the heterostructure improves the photo-transistor action.

Sensitivity Gains in Chemosensing by Lasing Action in Organic Optoelectronic Structures

A. Rose, C. Madigan, J. Ho, T. Swager, V. Bulovic
Sponsorship: NASA, ISN, NSF-MRSEC

Societal needs for greater security require dramatic improvements in the sensitivity of chemical and biological sensors for weapons detection. To meet this challenge, increased attention has been directed at materials and devices with highly non-linear characteristics. Semiconductive organic polymers (SOPs) (Figure 1) exemplify a class of amplifying materials which have also been recognized as promising lasing materials, although their susceptibility to optical damage due to photo-oxidation has thus far limited applications.

We recently demonstrated that for photostable SOPs, attenuated lasing in optically-pumped SOP thin films can exhibit more than 30-times higher sensitivity to explosive vapors than can be observed from spontaneous emission [1]. Through optical pumping, amplified stimulated emission was readily observed at sufficiently low pump power so as to prevent SOP bleaching during operation in ambient air. Ambient operation is necessary for applications involving the detection of explosives in the field. Upon exposure of the lasing SOP thin film to vapors of 2,4,6-trinitrotoluene (TNT) and 2,4-dinitrotoluene, cessation of the lasing action is observed and recorded. Associated enhancement of sensitivity is most pronounced when the films are pumped at intensities near their lasing threshold (Figure 2). The responses at low analyte-exposure levels are detectable in the lasing peak before any attenuation appears in the spontaneous emission peak. The strong binding of these nitro-aromatic analytes to electron-rich SOPs and their ease of reduction produce a selective response that is relatively immune to other airborne analytes (no response was observed upon exposure to benzene or naphthalene). Present efforts focus on incorporating SOPs into open, high-Q, optical-feedback structures that will reduce the lasing threshold as well as enhance sensitivity by using thinner active layers.
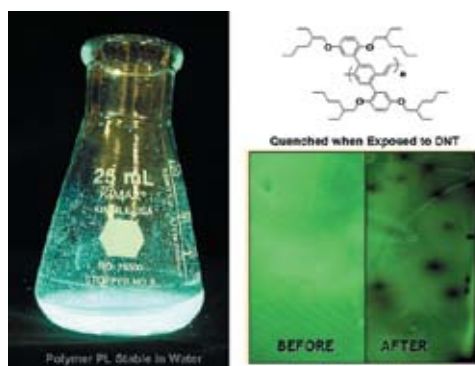

Figure 1: Fluorescence of the SOP in solution and in a thin film (before and after DNT exposure).
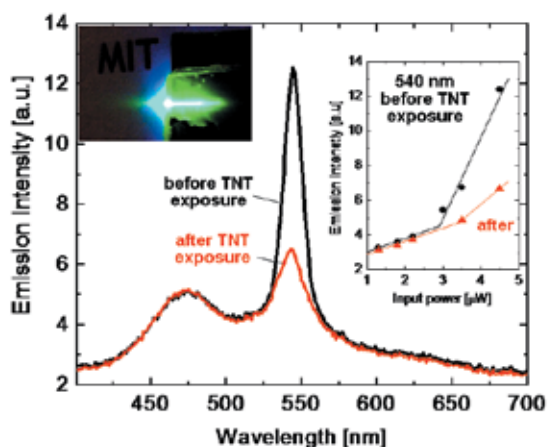
Figure 2: Spectral response of a ring-mode structure consisting of a 25-um-diameter, silica fiber dip-coated with an SOP thin film. The ASE attenuation in the absence of spontaneous emission attenuation after 1.5 min of exposure to saturated TNT vapor pressure. Right inset, plots of ASE peak-emission intensity (wavelength of 535 nm) as a function of excitation power. Left inset pictures a chemo-sensitive SOP thin-film laser.

REFERENCES:

[1] Rose, A., Z. Zhu, C.F. Madigan, T.M. Swager, V. Bulovic, "Sensitivity Gains in Chemo-sensing by Lasing Action in Organic Polymers," *Nature*, 434, 876 (2005).

Photovoltaics and Thermophotovoltaics

D.T. Danielson, T.M. Montalbo, T. Lin, L. Dal Negro, Y.Yi, K. Wada, L.C. Kimerling
Sponsorship: Shin-Etsu Chemical Corp.

This research program aims to design and prototype a novel photonic microstructure, in conjunction with thin silicon solar cells in order to enhance cell efficiency. The structure should increase the optical path length of wasted photons by creating anomalous refraction effects. We have proposed three-dimensional photonic crystal backside reflectors to achieve the strong bending of the incident light. The fabrication of regular arrays of air macro-pores in silicon (Si) has been achieved by electrochemical etching using DMSO-HF solutions on p-type Si substrates, affording the design advantages of higher solar cell base minority carrier diffusion lengths relative to n-type Si. The strong advantages of our new DMSO etching process are clearly displayed in Figure 1, showing a cross-sectional SEM of our recent porous samples. A depth of 22μm with average pore diameters of approximately 1.6μm was achieved indicating an impressive aspect ratio of ~14. As expected, lateral etching appears to have been suppressed and inter-pore walls are significantly thicker with respect to the samples produced by standard HF/ethanol processes. Additionally, a vertical pore growth rate 15 times greater than that achieved with ethanol as a solvent was achieved, making this process much more amenable to a realistic production environment.

We have successfully fabricated ordered high-aspect ratio macropores in p-type Si with ~1-2μm diameters and relatively thick pore walls through electrochemical anodization. This achievement represents a critical step toward the realization of 3D photonic structures directly integrated on the backside of a p-type Si solar cell to achieve strong light trapping for high-efficiency thin-film Si solar cells.
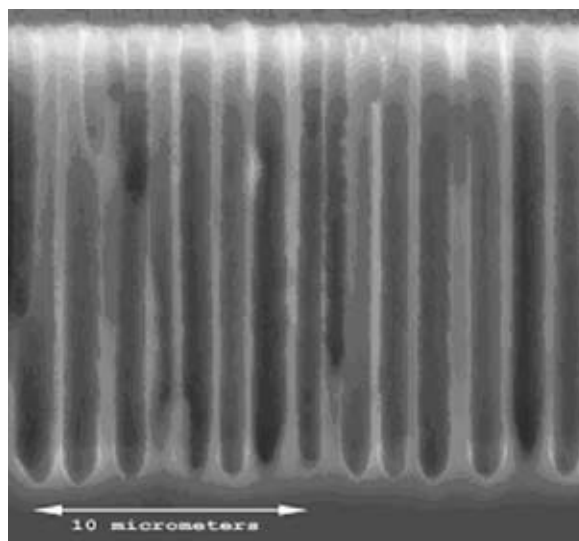
Figure 1: Cross-section SEM image of 30min, 4M HF/DMSO, 15mA/cm² porous Si sample

REFERENCES:

[1]   Danielson, D.T., T. Lin, T.M. Montalbo, L. Dal Negro, Y.Yi, K. Wada, and L.C. Kimerling, "Superprism Backside Reflector for Thin Crystalline Silicon Solar Cells," 14th Workshop on Crystalline Silicon Solar Cells & Modules: Materials and Processes, p. 273., NREL Report BK-520-36622 (2004).

[2]   Danielson, D.T., L. Dal Negro, Y. Yi, T. Lin, T. Montalbo, K. Wada, and L. Kimerling, "Three-Dimensional Photonic Crystal Backside Reflector for Efficient Light Trapping in Thin Crystalline Silicon Solar Cells," Proceedings of DOE solar program review meeting, October 24-28 (2004)

Concepts and Devices for Micro-scale, Thermo-photovoltaic Energy Conversion

H.K.H. Choy, C.G. Fonstad, Jr., in collaboration with R. Dimatteo (Charles Stark Draper Lab)
Sponsorship: Charles Stark Draper Laboratory

The first-order proximity-enhancement of thermo-photovoltaic energy conversion that we and CSDL demonstrated for the first time several years ago [1, 2] leads to a dramatic and important increase in energy conversion rate but only a modest increase in the efficiency of the conversion process. The challenge we are addressing now is to use the micro-scale geometry (in which the hot and cold surfaces are in extreme proximity) to increase the efficiency of thermo-photovoltaic energy conversion as significantly as we have increased the conversion rate.

Our work supports the C. S. Draper Laboratory (CSDL) effort on micro-scale thermo-photovoltaic (MTPV) electrical power sources. We have provided InAs-based MTPV cells to the CSDL effort; we have analyzed the impact of the enhancement effect on TPV cell performance; and we have evaluated more sophisticated, quantum-effect-based phenomenon that can be used to enhance significantly the energy selectivity of the energy transfer, and thereby dramatically increase the efficiency of the thermal to electrical energy conversion. We

have most recently also begun work on dot-junction, back-side-illuminated solar cells. In the past year we have designed an original InGaAlAs-on-InP heterostructure suitable for fabricating high performance dot-junction, back-side illuminated solar cells shown in Figure 1, and proposed an accompanying fabrication sequence. Referring to Figure 1, the uppermost n+ InGaAs layer is the n-side of the junction and a low-resistance contact layer. The InGaAlAs layers shield the minority carriers created in the wide, p-type InGaAs light-absorbing layer from surface recombination; the composition of this layer is graded to eliminate any barrier to electron flow from the absorbing layer to the n-side of the junction. The lowest p+ InGaAs layer reduces resistance as carriers flow laterally to ohmic contacts made to the p-side of the junction. The first sample of this heterostructure has been grown and CSDL researchers are doing fabrication and testing of the first set of devices.

n+ InGaAs contact layer and diode n-side (0.1 μm)

p- graded composition InGaAlAs layer (0.25 μm)

p- InGaAs absorbing layer and diode p-side (3.0 μm)

p+ InGaAs lateral current spreading layer (0.2 μm)

Semi-insulating (undoped) InP substrate
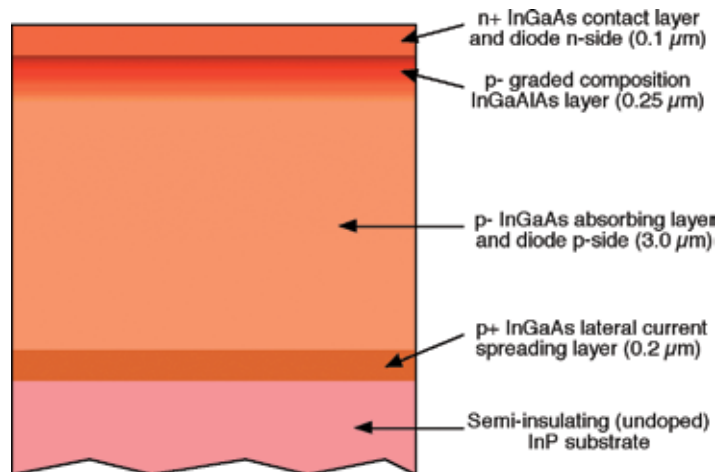
Figure 1: The layer structure for dot-junction, back-illuminated TPV and MTPV cells

REFERENCES:

[1] DiMatteo, R.S., P. Greiff, S.L. Finberg, K.A. Young-Waithe, H.K.H. Choy, M.M. Masaki, C.G. Fonstad, Jr., "Enhanced Photo-generation of Carriers in a Semiconductor via Coupling Across a Non-Isothermal Nano-scale Vacuum Gap," *App. Phys. Lett.* 79, 2001 pp. 1894-1896, 2001.

[2] Pan, J.L., H.K.H. Choy, C.G. Fonstad, Jr., "Very Large Radiative Transfer over Small Distances from a Black Body for Thermo-photovoltaics," *IEEE Trans. Electron Dev.*, vol. 47, pp. 241-249, 2000.

Nanoscale, Thermal-Imaging Microscopy

P. Mayer, D. Lueerssen, J. Hudgings, R.J. Ram
Sponsorship: ONR, NSF

Thermo-reflectance microscopy is a widely used means of measuring surface temperature changes that does not require physical contact of the surface (as opposed to the use of thermocouples, for example) combined with a better spatial resolution than IR thermography. A few years ago, Grauby et al. presented a break-though idea that improved the usability of CCDs two-dimensional detection [1]. However, the literature reveals a widespread belief that the temperature resolution of thermo-reflectance is limited to the order of 1K to 0.1. This conclusion stems from the assumption that a typical 12-bit CCD can measure a reflectivity of $R \leq 2^{12} = 4096$. At best, the measurable changes are equal to the quantization limit, $\Delta R = 1$. Under idealized circumstances (e.g., no noise),

the obvious conclusion is that the resolution of the system is $\Delta R/R = 2.5 \cdot 10^{-4}$. Intuition suggests that if we include the unavoidable shot noise, the resolution of $\Delta R/R$ can only be worse, but this conclusion is wrong. The resolution is, in fact, better than in the idealized case, and we demonstrate that $\Delta R/R$ can be measured with an uncertainty better than $1 \cdot 10^{-7}$. We utilize noise-induced level-crossing to measure changes in the thermoreflectance better than the limit of quantization of the camera. Using 467-nm light on gold, we have realized 10 mK temperature resolution simultaneously with 250-nm spatial resolution [2].
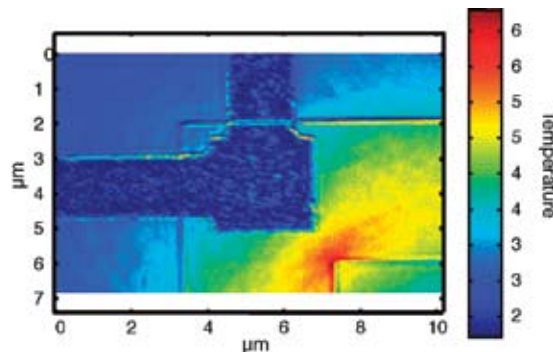
Figure 1: Thermal image of a diffused- Ssilicon resistor. The image shows the excess Joule heating in the inside corner of the resistor.
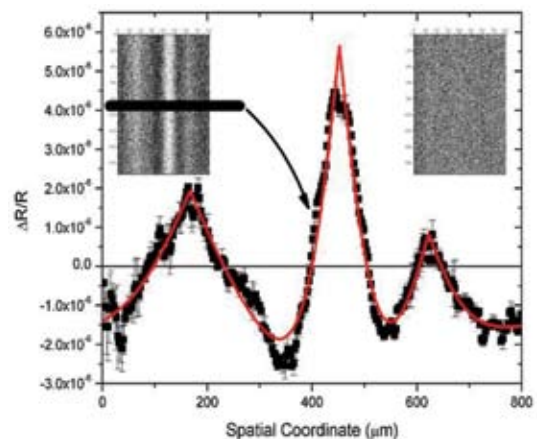
Figure 2: Heating due to non-radiative recombination at defects within a Ssilicon solar cell. The signal level is three orders of magnitude below the CCD-quantization limit.

REFERENCES:

[1] Grauby, S., B. C. Forget, S. Hole, and D. Fournier, "High resolution photothermal imaging of high frequency phenomena using a visible charge coupled device camera associated with a multichannel lock-in scheme," *Review of Scientific Instruments*, vol. 70, pp. 3603-3608, 1999.

[2] Lueerssen, D., J.A. Hudgings, P. Mayer, and R.J. Ram, "2D stochastically resonant thermo-reflectance microscopy with 700nm spatial and 25mK temperature resolution" *SemiTherm*, San Jose California, 2005.

Digital Holographic Imaging of Microstructured and Biological Objects

J.A. Dominguez-Caballero, J.H. Milgram, G. Barbastathis
Sponsorship: MIT Sea Grant

Digital Holographic Imaging (DHI) is a powerful technique that allows three-dimensional imaging by recording the optical-wave field using a CCD array. This recording is followed by a numerical reconstruction of the image field. The DHI is being employed to characterize micro-structured and biological objects at distances relatively far from the CCD with high lateral resolution. The amplitude and phase information can be retrieved from the reconstructed field, allowing us to obtain a more complete description of the sampled object.

The digital hologram is created by capturing the interference between the wavefronts scattered by an illuminated object and a reference beam. The intensity registered at the CCD plane is given by: $I_{CCD} = |r+o|^2$

where r is the reference field and o is the Fresnel diffracted-object field. The recorded intensity is then multiplied by the digitally generated version of the reference beam (r_D) in order to recover the virtual image. The next step is to reconstruct the object in the image plane by using the diffraction integral. The reconstruction is achieved using the convolution approach:

$$T_o = F^{-1}[F(I_{CCD} \cdot r_D) \cdot F(h)],$$

where T_o is the reconstructed field in the image plane; the operators $F\{\}$ and $F^{-1}\{\}$ are the forward and inverse Fourier Transforms, respectively, and h is the diffractive kernel. The reconstruction is optimized by using the Fast Fourier Transform algorithms.

Experiments using an in-line configuration reconstructed a USAF 1951 resolution target and a live brine shrimp. The recordings were made using a He-Ne Laser with $\lambda = 632.8$nm. The beam was expanded and split into two paths of equal length, forming a Mach-Zehnder Interferometer. The sampled object was placed in one of the paths and the other path was left clear to form the reference wave. Neutral Density Filters were used to control the relative intensity between the object and reference beams. The hologram was captured using a CCD array of 4096x4096 pixels with a pixel size of 9μm and a fill factor of 100%. Figure 1 shows the reconstruction made for the USAF 1951 resolution target located 15mm away from the CCD array. Figure 2 shows the reconstruction made for the live brine shrimp located at a distance of 167mm. The length of the brine shrimp is, approximately, 5mm.
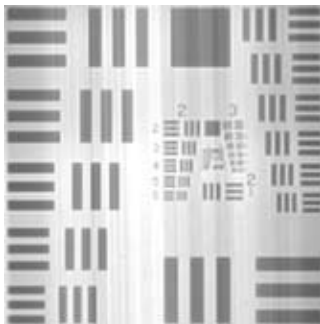

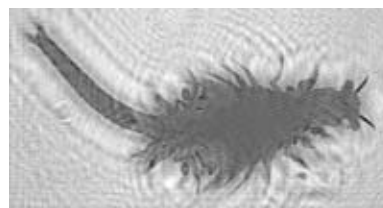Figure 1: Reconstruction of a USAF 1951 resolution target: z = 15mm.

Figure 2: Reconstruction of a live brine shrimp: z = 167mm.

Super-resolution Optical Profilometry Using Maximum-likelihood Estimation

W. Sun, G. Barbastathis, in collaboration with M.A. Neifeld (University of Arizona)
Sponsorship: Montage Program, DARPA

Highly precise and accurate profile measurement is important in various kinds of precision engineering, such as precise parts manufacturing, optical element grounding and polishing, etc. Several techniques have been developed for high-resolution profilometry in different application areas. We presented a number of volume-holographic imaging (VHI) based profilometery systems recently. The VHI-based profilometer optically slices the object to be measured layer-by-layer, and then the acquired raw images from each layer are sent to a computer. The computer reconstructs the 3-D profile of the object. The plane wave reference volume-holographic imaging (PR-VHI) based system with active monochromatic illumination can achieve $\approx$ 2 mm depth resolution at a 50 cm working distance. For stepwise object metrology, the resolution can be improved to $\approx$ 50µm at the same working distance. In this report, we present Viterbi Algorithm (VA) based maximum likelihood estimation data processing method for PR-VHI profilometry with multiplexing holograms. The method can resolve object's features at 8 different depth layers with 4 times super-resolution with raw images captured at only one lateral scanning process.

The experimental demonstration of the VA-based, super-resolution VHI profilometry was applied to a plastic LEGO® model. We set the VHI profilometer at the working distance at 50cm. To demonstrate the super-resolution, we deliberately closed down the aperture to degrade the nominal depth resolution to 6.5mm. The active illumination is from a Coherent Verdi®-5 Nd:YAG laser operated at 532nm. We repeated the experiments at the laser output powers of 25mw, 15mw, and 8mw to test the super-resolution performance at different SNR levels. Two multiplexing holograms recorded in a single $LiNbO_3$ crystal were used in the experiment. These two holograms were [consistent tense for experiment] focused on two different depth layers with the spacing of 6.4mm, equivalent to four LEGO® layers. In the profilometery process, the two holograms were set to focus on the 3rd and 6th layers of the LEGO® model (with distances z_1 and z_2 from the PR-VHI system, as shown in Figure 1). With mechanical scanning only at one lateral dimension (x direction shown in Fig. 1), two raw images of the profilometry slices at the 3rd and 6th layers of the LEGO® were acquired. These two slices were then sent to the VA based, post-processing to reconstruct the object. Figure 2 shows reconstructed LEGO models with the VA-based method and cross-correlation-based method . The results show that the VA-method generates a reconstruction almost without error.
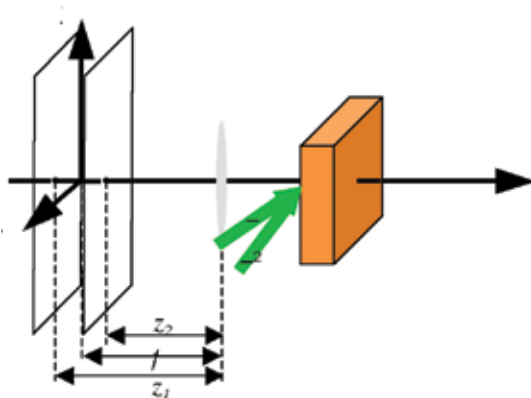

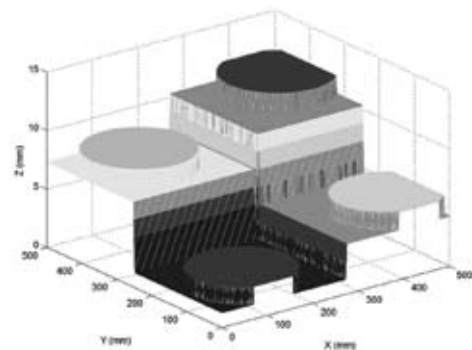Figure 1: Schematics of the PR-VHI super-resolution experiment with multiplexing holograms.

Figure 2: Reconstructed LEGO® model with VA-based post-processing method.

White-light Optical Profilometry at Long Working Distances

W. Sun, G. Barbastathis
Sponsorship: AFOSR, DARPA

We devised a real-time, optical profilometry technique with rainbow-illuminated, volume-holographic imaging (RVHI), as shown in Figure 1. A white light source is first analyzed by a diffraction grating and the object is illuminated by the decomposed rainbow. After passing through a cylindrical lens, the rainbow is focused to the focal plane of a volume holographic lens [a volume holographic lens is a specifically designed volume hologram acting as a lens but with unique optical properties]. The diffraction grating, cylindrical lens, and the objective lens are chosen in so that the rainbow projection on the focal plane satisfies the following coupled angular-wavelength shifting relation [1]:

$$\frac{\Delta\lambda}{\lambda} \approx -\frac{\Delta\theta}{\theta_s}$$

Where λ is the recording wavelengthand $\Delta\theta$ is the desired angular shift to the optical axis of a color component in the rainbow, which has a wavelength shift $\Delta\lambda$. Therefore, all the in-focus points along the x dimension are matched; in the y dimension they are also Bragg matched because of degeneracy. Thus, the entire rainbow plane is Bragg matched, resulting in a broad field of view (FOV). When shifted out of focus, each point source in the rainbow becomes Bragg mismatched due to defocus, much as a narrow-band source at the same wavelength would [2]. With wide FOV, RVHI can map the height of a reflective object across the entire lateral frame at one shot, without additional scanning. For better accuracy, images of different depth layers can be captured and mapped to different sections of the camera plane by multiplexing holograms [3].

RVHI can be set up in an inclined scheme to further improve depth resolution for profilometry of step-wised objects at a long working distance [4]. The target object (micro-turbine, see Figure 2(a)) is placed 450mm away. Figure 2(b) and (c) show two raw images of a micro-turbine acquired by RVHI at the top surface and the substrate, respectively.
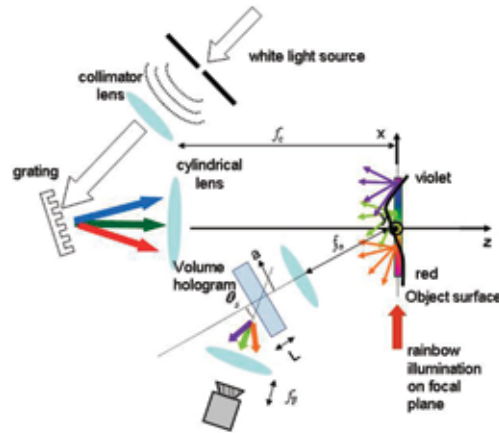
Figure 1: Illustration of rainbow volume holographic imaging system.
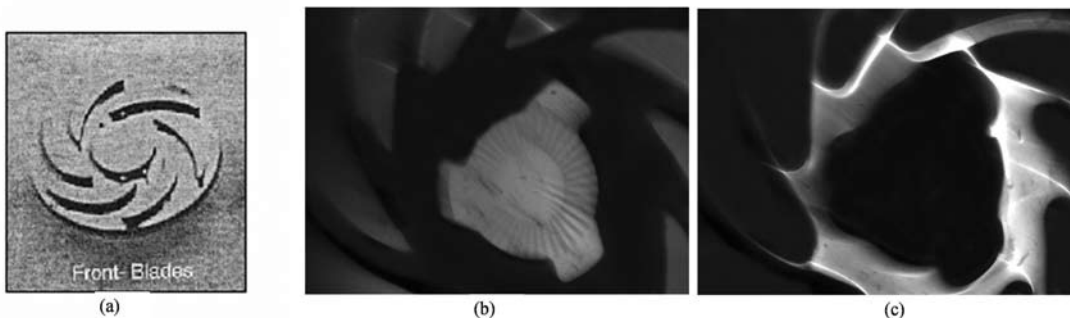
Figure 2: Image acquisition using RVHI: (a) object illuminated with rainbow; (b) and (c) raw images showing depth-selectivity across the rainbow field.

REFERENCES:

[1]   Barbastathis, G. and D. Psaltis, "Shift-Multiplexed Holographic Memory Using The Two-Lambda Method," *Opt. Lett. 21*. pp. 432-434, 1996.

[2]   A. Sinha, A., W. Sun, T. Shih, and G. Barbastathis, "Volume Holographic Imaging in Transmission Geometry," *App. Opt. 43,* pp. 1533-1551, 2004. [use lower-case letters in journal article as consistent with [1], [3], & [4]

[3]   Liu, W., D. Psaltis, G. Barbastathis, "Real-time Spectral Imaging in Three Spatial Dimensions," *Opt. Lett., 27,* pp. 854-856, 2002.

[4]   Sinha, A. and G. Barbastathis, " Volume Holographic Imaging for Surface Metrology at Long Working Distance," *Opt. Exp. 11*, pp. 3202-3209, 2003.

Optical Measurement of 3-D Deformation in Transparent Materials

K. Tian, T. Cuingnet, Z. Li, W. Liu, D. Psaltis, G. Barbastathis
Sponsorship: Montage Program

Deformation of volume holograms, such as shrinkage during processing [1], can cause deviation in the angle or wavelength for the Bragg matching condition [2], and aberrations in the reconstructed image. This problem, usually associated with the investigation of holography materials, has received much attention. The deformation models used in the literature are relatively simple, since their target is simple linear deformation. In this paper, we present a generalized theory that can deal with arbitrary deformations. We derived a general expression of the response of a volume grating to arbitrary deformation,

using a perturbative approach. We constructed experiments, as shown in Figure 1, to measure the effect of the deformation due to a point-load exerted normally on the surface of a hologram on the diffracted field from both plane-wave transmission and reflection hologram. The experiment results, as Figure 2 shows, are consistent with the theory. Using this technology, we can determine the deformation itself, based on a set of observations of the field diffracted from a known (pre-deformation) volume hologram.
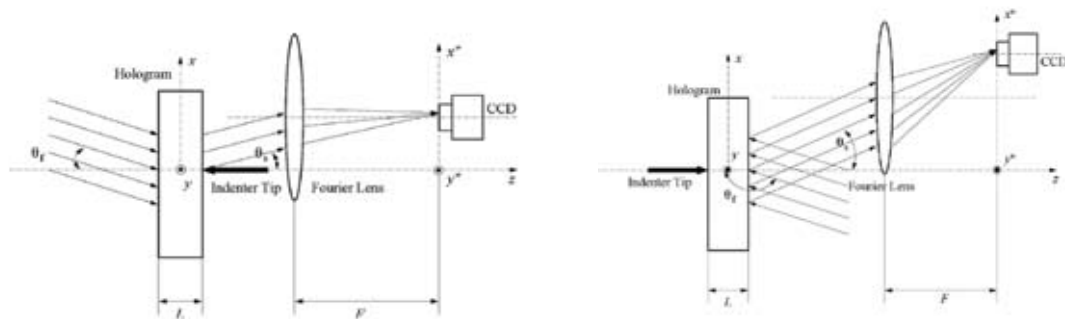
Figure 1: Experimental geometry when a point load is exerted on (a) a transmission- hologram; (b) a reflection hologram

(a)   (b)

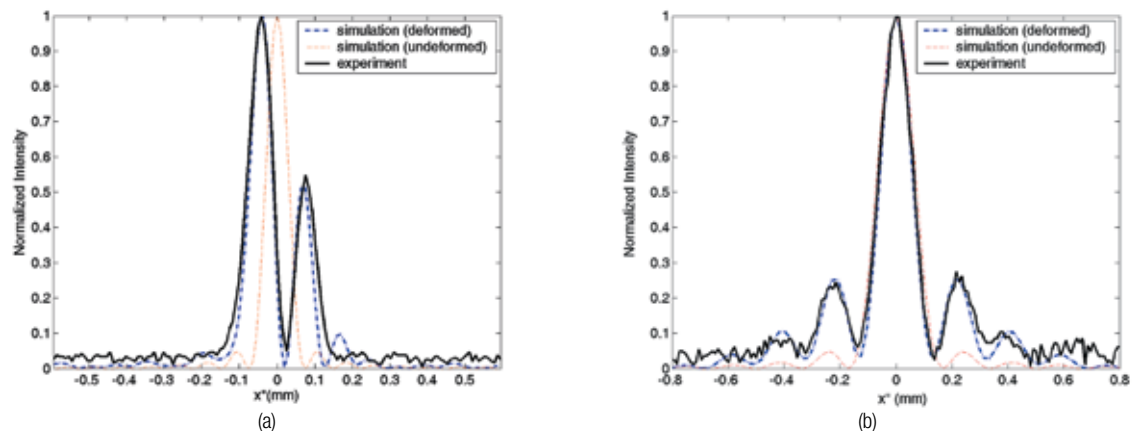Figure 2: Experimental and simulated results when a point load is exerted on (a) a transmission type hologram and (b) a reflection type hologram

REFERENCES:

[1]   Colburn, W.S. and K.A. Haines, *Appl Opt,* 10, pp.1636-1641, 1971; B.L. Booth *Appl Opt.,* 14, pp. 593-601, 1975.
[2]   Hariharan, P., Optical Holography: Principles, Techniques, and Applications. Cambridge: Cambridge University Press, 1984.

Light Emitting Aperiodic Photonic Structures

L. Dal Negro, J.H. Yi, V. Nguyen, Y. Yi, J. Michel, L.C. Kimerling
Sponsorship: NSF-MRSEC

The control of light-matter interactions in complex dielectrics without translational invariance offers the ultimate potential for the creation and manipulation of light states. Unlike periodically arranged dielectrics (photonic crystals), aperiodic dielectric arrays show unique light localization and transport properties related to the lack of translational symmetry, and an unprecedented degree of structural complexity. Aperiodic dielectrics can be deterministically generated following simple mathematical rules. They offer significant advantages over randomly generated non-periodic materials in terms of reproducibility, processing, and design. Recently [1,2] we fabricated the first light-emitting silicon-rich, SiN_x/SiO_2 Thue-Morse (T-M) multilayer structures in order to investigate the generation and transmission of light in strongly aperiodic deterministic dielectrics. Photoluminescence and optical transmission data experimentally demonstrate the presence of emission-enhancement effects occurring at wavelengths corresponding to multiple T-M resonance light states. The unprecedented degree of structural flexibility of T-M systems can provide alternative routes towards the fabrication of optically active, multi-wavelength photonic devices.
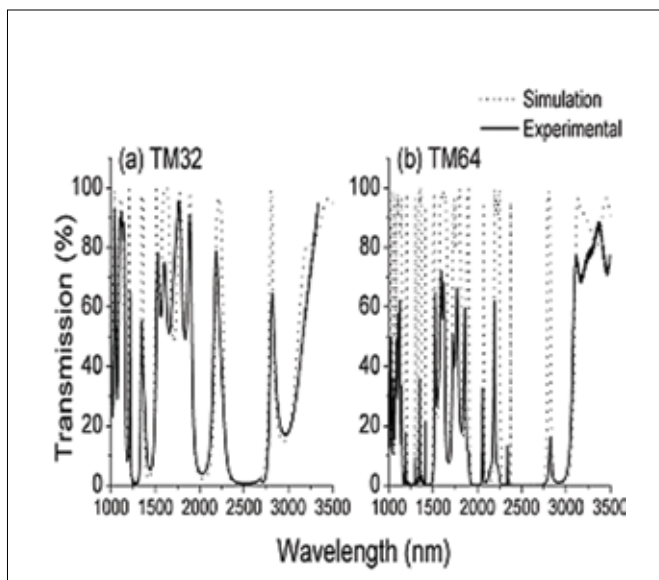
Figure 1. (a) Experimental (solid line) and calculated (dotted line) transmission for the 32-layer T-M structure (TM32); (b) Experimental (solid line) and calculated (dotted line) transmission for the 64-layer T-M structure (TM64). For all the simulations we have considered n_A=2.23 (SiN_x), n_B=1.45 (SiO_2). The thickness simulation parameters that yield the best fit with the experimental transmission data are d_A=198.9 nm and d_B=273 nm, which are approximately 6% thicker and 4% thinner than the targeted values defined by the Bragg condition at l_0 =1.65 mm.
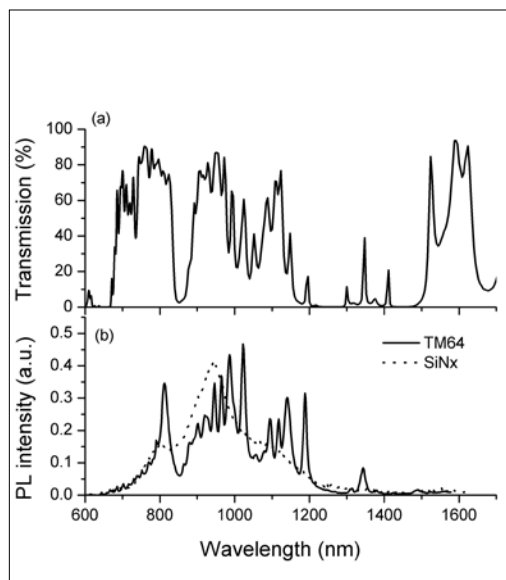
Figure 2. (a) Experimental transmission for the 64-layer T-M structure; (b) Comparison of the room-temperature TM64 emission spectrum and the homogeneous SiN_x -reference-sample emission spectrum . The pump power was 5mW.

REFERENCES:

[1]   Dal Negro, L., J.H. Yi, V. Nguyen, Y. Yi, J. Michel and L.C. Kimerling, "Light Emission in Aperiodic Thue-Morse Dielectrics*," Proceedings of MRS*, 92331, F1.3 2005.

[2]   Dal Negro, L., J.H. Yi, Y. Yi, V. Nguyen, J. Michel, L.C. Kimerling, "Spectrally Enhanced Light Emission from Aperiodic Photonic Structures" accepted for publication, *Appl. Phys. Lett.*, 2005 .

Photonic Crystals

L. Zeng, Y. Yi, C.-Y. Hong, X. Duan, L.C. Kimerling
Sponsorship: National Renewable Energy Laboratory (NREL), CMSE

In order to improve thin film solar cell efficiency, it is important to enhance the optical path length by trapping light in the cell. We have successfully developed a new light-trapping scheme, which combines a reflection grating in the substrate with a distributed Bragg reflector (DBR). It can enhance optical path length by more than 10^4 times with little loss of reflection. Consequently, incident light can be almost completely absorbed. In turn, we expect the quantum efficiency of the solar cell based on our photonic structure to be improved significantly.

In the year 2004, we achieved rapid progress in several aspects:

- We have fabricated high-quality DBRs with extremely high reflectivity that agrees well with simulation. For instance, using 5 pairs of Si/Si_3N_4 gives a reflectivity of 99.6%, whereas that for Si/SiO_2 is 99.98%.

- We have successfully developed a practical fabrication process for the silicon grating DBR by the following steps: first, optical projection lithography is used to pattern the Si substrate into gratings with periods on the order of wavelength; then a plasma etch is used to accurately control etch-depth; the last step is to deposit DBR stacks using LPCVD or DCVD. Figure 1 is the SEM image of Si grating with one pair of Si_3N_4/Si.

- Our Si grating displayed strong light bending effects (Figure 2). We have set up a measurement system that has a tunable-wavelength laser source and a detector that can be rotated over 180 degrees, allowing accurate determination of the reflected light direction and intensity.

The next step is to integrate the new back-reflector with simple solar cells to verify cell-efficiency improvement.

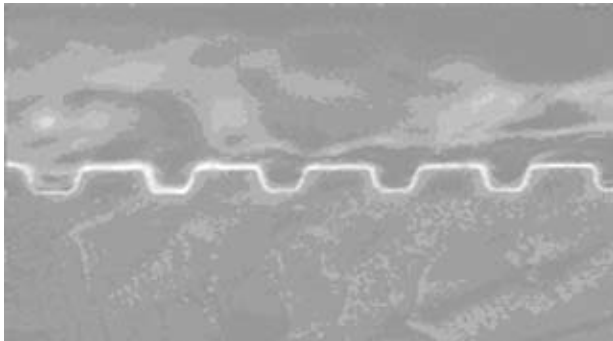Figure 1: An SEM image of a Si grating with one pair of Si_3N_4/Si
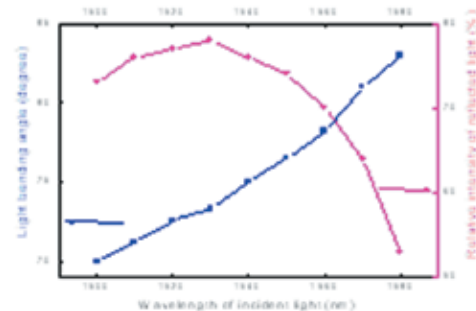

Figure 2: Optical measurement results of the Si grating.

REFERENCES:

[1]   Hamakawa, Y. (Ed.), Thin-Film Solar Cells, Next Generation Photovoltaics and its Applications, Springer, Berlin; New York , 2004.
[2]   Green, M.A., Silicon Solar Cells, Advanced Principles & Practice, University of New South Wales, Sydney, Australia, 1995.

Electrically-Activated Nanocavity Laser Using One-Dimensional Photonic Crystals

E. Mattson, G.S. Petrich, L.A. Kolodziejski, S. Assefa
Sponsorship: NSF-MRSEC

In the future, optical networks may play an expanded role not only in telecommunications, but also in computers and other common electronic devices. These optical networks will require small, on-chip light sources. Using the photonic crystal's ability to strongly confine light, photonic crystal lasers are both very small and efficient, making them ideal for integration into photonic integrated circuits. The laser is very flexible in that simply by changing the active material or by changing the size and spacing of the holes that create the photonic crystal, the emission wavelength can be varied. This laser should be more efficient than current light sources from the standpoints of both the energy and chip design, and should represent a major improvement in on-chip light sources.

The laser consists of two one-dimensional photonic crystal waveguides that cross each other (Figure 1). The laser's nanocavity, which has a length of ~1 µm, is located where the defect regions of the two photonic crystal waveguides overlap.

The bottom waveguide consists of an active layer containing InGaAs quantum dots, which emit at 1300nm, sandwiched between two GaAs and AlGaAs layers. Once the photons are generated in the nanocavity, the light will be confined laterally and vertically, by index of refraction changes at the materials' interfaces. However, at the two ends of the waveguide, a series of holes are etched, forming the photonic crystal, which confines the light lengthwise in the nanocavity. Some of the light will leak into the upper InGaAlP waveguide. The upper waveguide exhibits less loss than the lower waveguide and has an asymmetric number of holes etched into it around the nanocavity, allowing the direction of the emitted light to be controlled. The entire photonic crystal part of the laser is about 5 µm square.
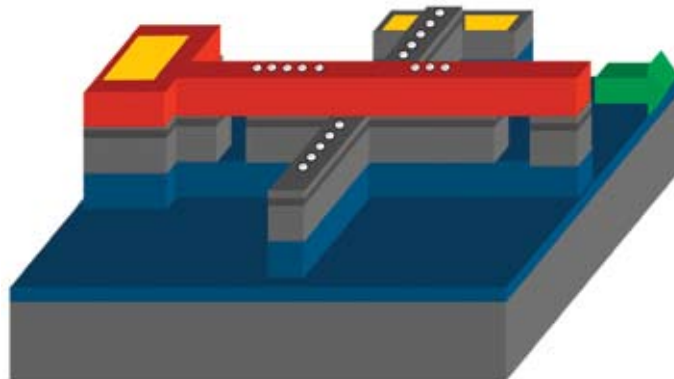

Figure 1: Depiction of the electrically-activated, photonic crystal nanocavity laser. The green arrow represents the direction and location of the emitted light.

Super-Collimation of Light within Photonic Crystal Slabs

S.N. Tandon, M. Dahlem, P. Rakich, M. Ibanescu, M. Soljacic, G.S. Petrich, J.D. Joannopoulos, E.P. Ippen, L.A. Kolodziejski

A super-collimator is a device in which light is guided by the dispersion properties of a photonic crystal slab rather than by photonic crystal defects or waveguiding structures. Photonic crystals form the essence of the super-collimation effect. The device, schematically shown in Figure 1, consists of a two-dimensional photonic crystal composed of a square lattice of cylindrical air holes etched into a high-index material. Furthermore, the photonic crystal occupies the entire surface of the super-collimator. The cleaved edges of the super-collimator function as input or output facets. The initial design has focused on realizing super-collimation at a wavelength of 1.44 μm.

Figure 2 shows images of a fabricated super-collimator using a silicon-on-insulator (SOI) wafer. The photonic crystal holes are patterned using interference lithography and are etched into the upper Si layer via reactive ion etching. The left inset of Figure 2 shows the full 1cm x 1cm device with its cleaved input and output facets. The photonic crystal occupies the full sample area and the SEM images at the center and right inset of Figure 2 show the details of the photonic crystal cross-section. The center image also illustrates the large area nature of the photonic crystal. The right inset shows that the air holes are etched through the upper silicon layer. The photonic crystal rests on a buried SiO_2 layer to minimize the coupling to the substrate.

Testing of the super-collimator device is in progress. Preliminary results show that the super-collimation effect is wavelength dependent, with the strongest collimation occurring at a wavelength of 1495 nm. Results also suggest that super-collimation can be sustained within the photonic crystal on millimeter-length scales with very little divergence.

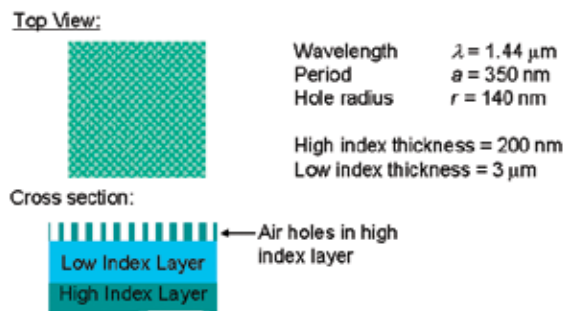Figure 1: Super-collimator device design showing the top and side views of the device.
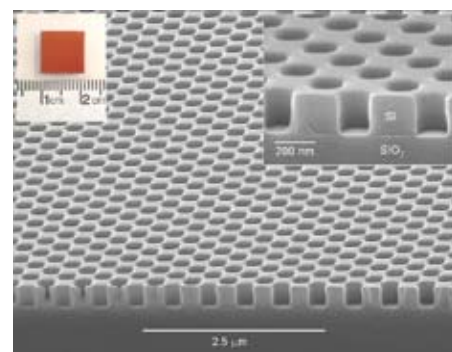

Figure 2: Images of the fabricated super-collimator device. Left inset: Digital photograph showing the full sample. Center: Scanning electron microscope (SEM) image showing the large area nature of the 2D photonic crystal. Right inset: SEM image showing a cross-sectional image of the device fabricated using a SOI wafer.

Diamond-Structured Photonic Crystals

M. Maldovan, E.L. Thomas
Sponsorship: ARO

Certain periodic dielectric structures can prohibit the propagation of light for all directions within a frequency range. These "photonic crystals" allow researchers to modify the interaction between electromagnetic fields and dielectric media, from radio to optical wavelengths. Their technological potential, such as the inhibition of spontaneous emission, enhancement of semiconductor lasers, and integration and miniaturization of optical components, makes the search for an easy-to-craft photonic crystal with a large band-gap a major field of study.

This progress article surveys a collection of robust complete three-dimensional dielectric photonic-band-gap structures for the visible and near-infrared regimes, based on the diamond morphology together with their specific fabrication techniques. The basic origin of the complete photonic band-gap for the "champion" diamond morphology is described in terms of dielectric modulations along principal directions. Progress in three-dimensional interference lithography for fabrication of near-champion diamond-based structures is also discussed.
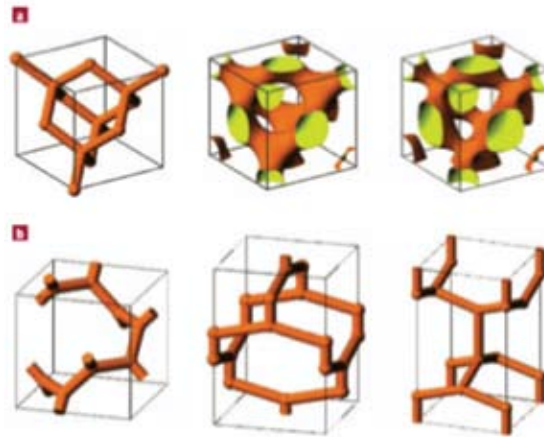
Figure 1: The level-set diamond D and three-connected diamond structures: (a, left): The rod-connected diamond. Center: The level-set diamond-D structure connects neighbor sites of the diamond lattice, producing a continuous dielectric network. This analytical representation allows the fabrication of the diamond morphology through the interference lithography technique; (right): The unbalanced diamond structure connects neighbor sites of the diamond lattice with different weights producing a continuous but unbalanced diamond network. This unique structure presents two simultaneous complete photonic band-[?]gaps for a wide range of volume fractions;(b):3-D representations of the unit cells for the three-connected diamond-like structures. The unit cell ratios are a:a:a, a:a:√2a, and a:a:√3a, respectively. The maximum gap values are 26.6%, 26.2%, and 22%.The structure on the right has both three- and four-connected nodes [40?].

REFERENCE:

[1]   Maldovan, M., Thomas, E.L., "Diamond-structured Photonic Crystals", *Nature Materials,* 3, 593-600, 2004.

Photonic Crystals through Holographic Lithography: Simple Cubic, Diamond-like, and Gyroid-like Structures

C.K. Ullal, M. Maldovan, E.L. Thomas, G. Chen, Y.-J. Han, S. Yang
Sponsosrship: AFOSR, ARO

We show how to fabricate three basic photonic crystal structures with simple cubic, fcc, and bcc translational symmetry by interference lithography. The structures are fabricable by the interference of beams launched from the same half space. The simple cubic structure is size-scalable while the structure with fcc translational symmetry possesses two band gaps. Both these structures are experimentally realized.
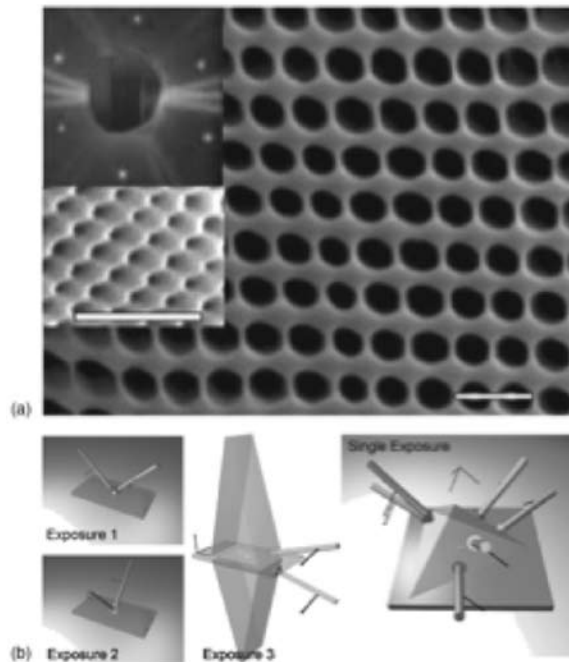
Figure 1: Surface and configuration of P-structure: (a) SEM micrograph of the (100) surface for a P-surface structure, with a periodicity of 1.1 μm. The inset shows a SEM image of a P-surface structure with a periodicity of 0.5 μm, demonstrating size scalability. The inset diffraction pattern comes from another P-surface structure showing the (111) orientation. The scale bars shown are 2 μm. (b) Two possible six-beam configurations for the fabrication of the P-structure. The polarizations are indicated as small arrows on the beams.

REFERENCE:

[1]   Ullal, C.K., Maldovan, M., Chen, G., Han, Y-J, Yang, S., Thomas, E.L., "Photonic Crystals through Holographic Lithography: Simple Cubic, Diamond-like, and Gyroid-like Structures", *Applied Physics Letters*, 84, pp. 5434-5436, 2004.

Three-Dimensional Network Photonic Crystals via Cyclic Size Reduction/Infiltration of Sea-Urchin Exoskeleton

Y.-H. Ha, R.A. Vaia, W.F. Lynn, J.P. Constantino, J. Shin, A.B. Smith, P. Matsudaira, E.L. Thomas
Sponsorship: Dupont-MIT Alliance, AFOSR

Many naturally occurring solids possess periodic structures that give rise to visible photonic crystal properties, commonly termed structural colors. Some stunning examples are butterfly wings (one-dimensional, 1-D), abalone shells (1-D), sea mouse spines (two-dimensional, 2-D), and natural opals(three-dimensional, 3-D). Exploitation of other periodic natural structures is, however, limited by the inherently large size scale and the low dielectric contrast of the materials. Furthermore, these generally more complex geometries are a challenge to model correctly in order to obtain correct band diagrams. Here we report the development of a high-fidelity, cyclic, size- reduction and infiltration scheme and apply it to a sea urchin exoskeleton to successfully fabricate a high-dielectric contrast, 3-D photonic crystal exhibiting a stop band in the mid-IR range. The band structure of the exoskeleton is modeled using level set mathematics and agrees well with the experimental reflectivity exhibited by the 3-D bi-continuous tellurium network of the replicated urchin.
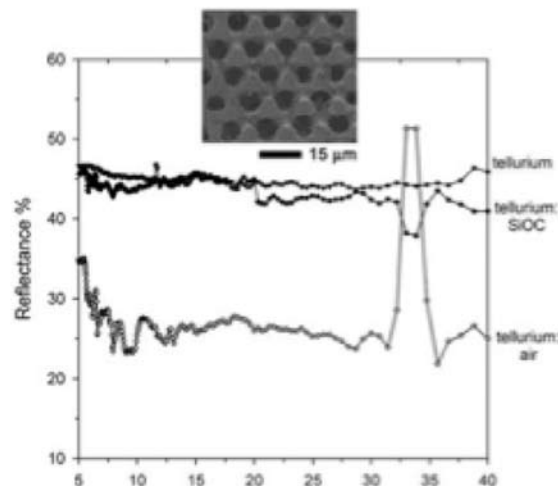
Figure 1: Reflectance spectra θ_i=20° of the bulk tellurium, tellurium: SiOC and tellurium:air replicas. The inset SEM image shows the three-fold symmetric (111) facet of the tellurium:air network after polishing and etching the tellurium:SiOC structure. The reflectivity peak from tellurium: air is centered at 34 μm.

REFERENCE:

[1]   Ha, Y.-H., Vaia, R.A., Lynn, W.F., Constantino, J.P., Shin, J., Smith, A.B., Matsudaira, P.T., Thomas, E.L., "Three-Dimensional Network Photonic Crystals via Cyclic Size Reduction/Infiltration of Sea Urchin Exoskeleton", *Advanced Materials*, 16, pp. 1091-1094, 2004.

Layer-by-layer Diamond-like Woodpile Structure with a Large Photonic Band Gap

M. Maldovan, E.L. Thomas, C.Carter
Sponsorship: Singapore-MIT Alliance, U.S. Army

A layer-by-layer, periodic dielectric structure with a large photonic band gap is presented. It consists of a layer-by-layer approximation to the triply periodic bi-continuous level set D surface structure having diamond (FD3m) symmetry. The structure retains the ease of fabrication of the standard woodpile while increasing the maximum quality factor of the gap by 28%. Photonic band gap properties of this structure were calculated using the plane-wave method and its band gap optimized at a fixed index contrast of 3.6.1.

Figure 1: Schematic three-dimensional representation for (a) spheres on a diamond lattice, (b) standard woodpile, (c) diamond-woodpile, and (d) bi-continuous, diamond D level set
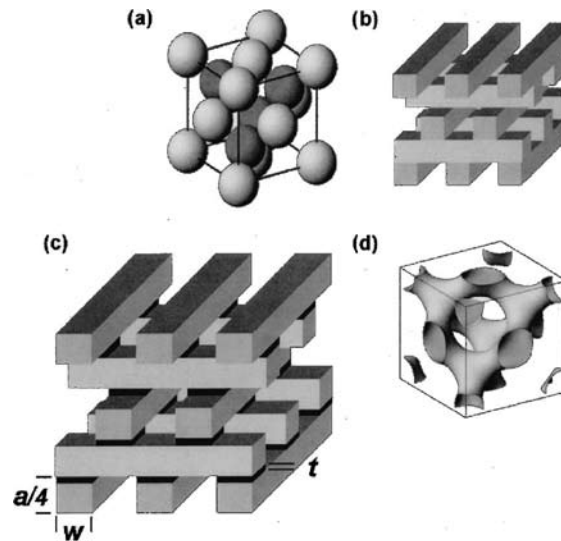
REFERENCES:

[1]   Maldovan, M., Thomas, E.L., Carter, W.C., "Layer-by-Layer Diamond-Like Woodpile Structure with a Large Photonic Band Gap," *Applied Physics Letters*, 84, pp. 362-364, 2004.

Localized, Guided Propagation Modes in Photonic Crystals with Shear Discontinuities

K. Tian, G. Barbastathis, in collaboration with J. Hong (Jet Propulsion Laboratory)
Sponsorship: Montage Program

Photonic crystals consist of periodic arrays of dielectric media [1,2]. Electromagnetic waves propagate in photonic crystals as Bloch waves whose coupling gives rise to the band structure, which may include forbidden gaps where the waves cannot propagate. Certain defects can lead to the coupling of energy to confined, localized states in the vicinity of the defect. We propose a new type of defect, consisting of a shear discontinuity in a photonic crystal lattice. Figure 1(a) shows a square lattice of circular dielectric columns with a shear discontinuity in the middle row. The circular dielectric columns in the middle line are cut in half. The shear shift is exactly half the lattice constant. Using FDTD, we simulated a band-limited pulse with its spectrum inside the band gap of the (unperturbed) photonic crystal being injected by the waveguide near the tip of the sheared slice. As Figure 1(a) shows, the entire pulse is well localized to the shear plane as it propagates in the crystal. The confined propagation mode occurs over a broadband spectrum. As Figure 1(c) shows, the coupling efficiency is almost 100% over a long wavelength range, provided that the shear shift is approximately half a lattice constant.

(a)

(b)

(c)
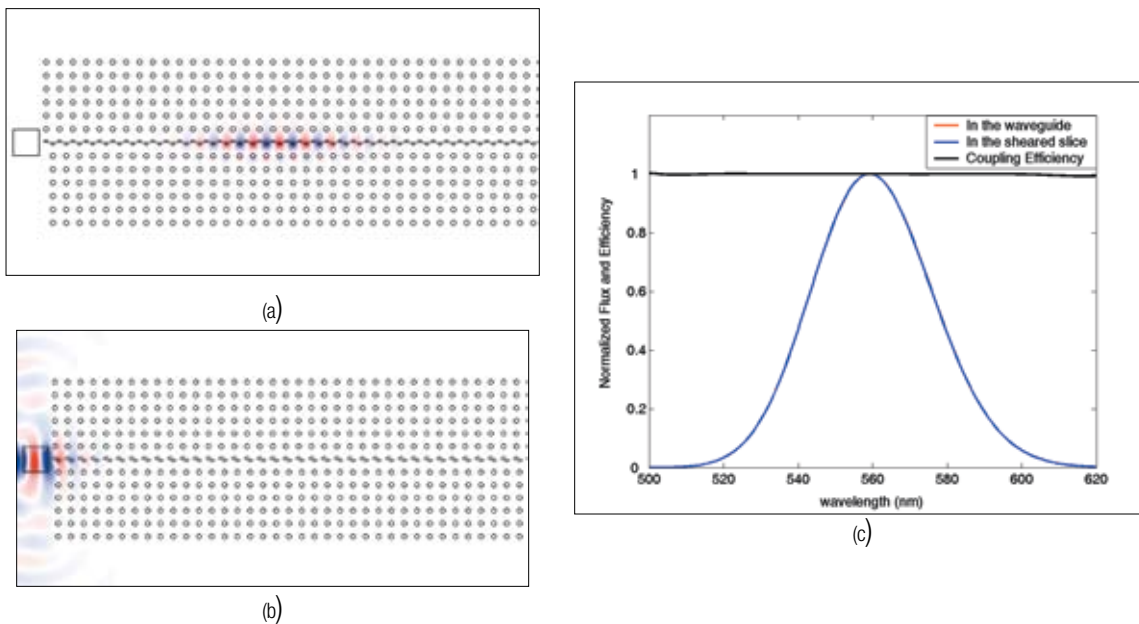
Figure 1. The pulse propagates inside the sheared photonic crystals. The refractive index of basis media is 1.0; that of the circular dielectric columns is 3.0. The diameter of each column is 80nm and the lattice constant is 200nm. The duration of the pulse is 10fs and its center wavelength is 560nm: (a) half-lattice-constant shift; (b) quarter-lattice-constant shift (the confinement is turned off); (c) the spectrum of flux at the exit of the waveguide and in the sheared slice and the couple-in efficiency of (a)

REFERENCES:

[1]   Ho, K.M., C.T. Chan, and C.M. Souloulis, *Phys. Rev. Lett.* 65(25) p. 3152,1990; E. Yablonovitch, T.J. Gmiter, and L.M. Leung, *Phys. Rev. Lett.* 67(17) p. 2295,1991; R. D. Meade, et al., *Phys. Rev. B.* 44(24) p. 13772 1990; W.M. Robertson etal., *Opt. Lett.* 18(7) pp. 528-530,1993.

[2]   Yeh, P., Optical Waves in Layered Media, New York: Wiley, 1988; J.D. Joannopoulos, R.D. Meade and J.N. Winn, Photonic Crystals: Molding the Flow of Light, Princeton, NJ: Princeton University Press, 1995.

Nanoelectromechanical Optical Switch for 1550 nm Light

R.E. Bryant, M.L. Povinelli, S.G. Johnson, G.S. Petrich, J.D. Joannopoulos, E.P. Ippen, L.A. Kolodziejski

One major objective of optical engineering research is to bring optical systems to the large-scale functionality of electrical systems. Striving to reach this objective, high-index-contrast, planar, evanescently coupled, Nano-Electro-Mechanical (NEM) waveguide switches using the GaAs-based material system are being developed.

The concept that is behind the NEMs switch combines two ideas: high-index-contrast waveguide optics and electromechanical actuation. High-index-contrast waveguide optics can route optical signals via waveguides with sizes of hundreds of nanometers in cross-section. Also, the evanescent method of energy transfer occurs along 100-nanometer coupling lengths and separations. The ability to exploit these length scales leads to a small device footprint, which lends itself to large-scale integrated optics. The physical dimensions of high-index-contrast evanescent coupling provide the impetus for the development of planar opto-electronic NEM systems. Furthermore, due to the size of NEM systems, it is possible to design switches with microsecond response times which would increase the number of potential applications for use by system designers that would not have been possible using the larger Micro-Electro-Mechanical-based switches.

A considerable amount of design and fabrication work has been invested in the development of the NEMS switch. Theoretically, when a voltage is applied to the switch, the two waveguides reduce their separation distance in order to achieve lateral evanescent coupling, which allows 100% of the optical energy to be transferred between the waveguides. In the initial, unbiased state, the initial separation distance prevents lateral coupling. Experimentally, GaAs-based waveguides with release lengths over 30 microns long have been achieved for waveguides that are 1-µm thick and ~300-nm wide, with excellent lateral and horizontal waveguide-to-waveguide alignment. Because the GaAs waveguides typically reside on thermally-oxidized GaAlAs layers, oxidation experiments have been performed to investigate the correlation between the resulting stresses that affect the waveguide at the point where the waveguide becomes suspended to the stoichiometry of the oxidized GaAlAs layer.

MEMS Switching for Integrated Optical Systems, Part (1): Fabrication

S. Takahashi, L. Waller, G. Barbastathis
Sponsorship: DARPA

Ring resonators are optical devices that can act as wavelength-specific add/drop filters, and they have important applications in optical add-drop multiplexers. These resonators can be switched on or off by use of a metal MEMS structure built above the ring resonator and actuated by electrostatic force, as shown in Figure 1. When the metal structure is pulled down to interfere with the evanescent field of the ring waveguides and cause loss, the device will lose its resonance, and hence, the filter will be switched "off." As the structure is freed from the electrostatic force and restored to its natural position above the evanescent field of the ring, the resonator will turn "on" and act normally as a filter. This MEMS structure is easily fabricated by a standard process (Figure 2). We are investigating the use of titanium nitride (TiN) as the material for the MEMS structure. Not only does TiN have appealing mechanical properties (e.g. high modulus-to-density ratio, high yield stress) and electrical conductivity, but a large body of knowledge also exists concerning its micro-fabrication techniques due to its wide use in CMOS fabrication, i.e., for diffusion barriers and local interconnects[1]. Therefore, TiN has high potential as a MEMS/NEMS structural material, especially for those applications that require electrostatic actuation of beams, bridges, etc.

One major problem in designing and fabricating this device is the residual stress of the MEMS structure, which could essentially deflect the beam vertically and allow the conductive structure to interfere with the evanescent field in the "on" state. Appropriately controlling the deposition parameters or annealing the material before its release from the sacrificial layer can control residual stress. Previous studies have shown that annealing of TiN by heating to 500°C and cooling back to room temperature at a rate of 2°C per minute can induce a significant reduction of stress in a TiN membrane. This MEMS switching device has a broad range of application in micro and nano-photonics, where the device can operate in the same fashion to interfere with the evanescent field of guided light, such as in photonic-crystal-based and plasmon-optics-based devices.
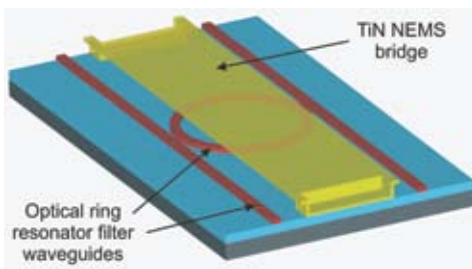

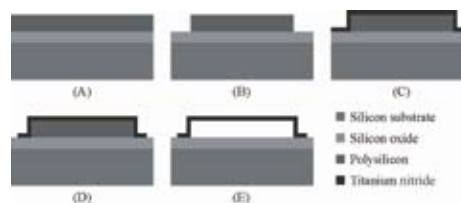Figure 1: Schematic of the MEMS ring resonator filter switch.

Figure 2: Fabrication process of the MEMS structure

REFERENCES:

[1]   Plummer, J.D., M. D. Deal, P. B. Griffin, *Silicon VLSI Technology*, Upper Saddle River, New Jersey: Prentice Hall, 2000.

MEMS Switching for Integrated Optical Systems, Part (2): Instrumentation and Control

L. Waller, S. Takahashi, G. Barbastathis
Sponsorship: DARPA

We have shown that wavelength-selective, integrated optical switches controlled via MEMS-actuation can be fabricated and operated. These devices have potential uses in optical networking, optical sampling, and RF- MEMS switching. However, practical application of these switches requires tuning of the dropped wavelength. To achieve this, we can use a dielectric MEMS bridge and control it in an analog fashion. If the dielectric bridge is moved vertically within the evanescent field of the ring resonator, the optical path length of the resonator, and thus the wavelength selected by the ring resonator, shift. In order to achieve tuning over one full wavelength channel of 30nm, we must control the MEMS bridge with a positional accuracy better than 0.7Å. Noise models for the device and control have been developed to predict the system noise, and a capacitive sensing feedback circuit is being designed to meet specifications (Figure 1). Capacitive sensing is a highly accurate, easily implemented feedback method that has shown to be useful in micro devices. The MEMS dielectric bridge can act as one electrode of a three-electrode capacitive sensor (Figure 1), in which a sensing signal and a control signal are applied to the outer two electrodes in order to displace the dielectric bridge to the desired height. Figure 2 also shows the response of this system to a two-pulse input. The device's performance can be measured, both temporally and spectrall,y using a lensed fiber to couple into and out of the integrated waveguides.
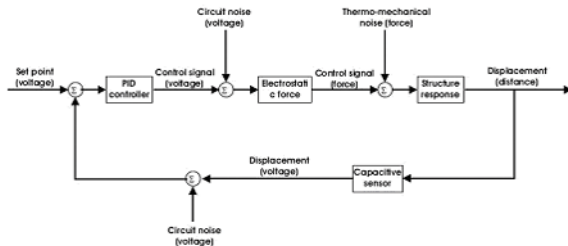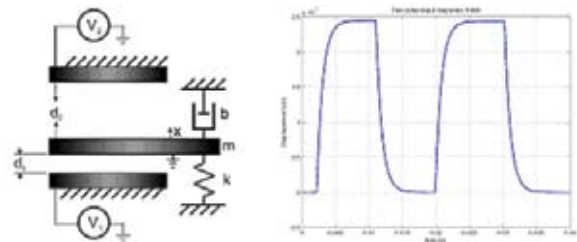

Figure 1: Flow chart for system model.

Figure 2: Three-electrode model and its [it's = it is]system response to pulses.

Techniques for Coupled Optimization and Simulation

K.C. Sou, J.H. Lee, J. Bardhan, L. Daniel, A. Megretski, Y. Avniel, S. Johnson, J. White
Sponsorship: MARCO IFC and GSRC, DARPA

The enormous advances in both interior-point-based, convex optimization and fast methods for three-dimensional simulation are making development of design tools that perform automatic structural optimization much more feasible. We are developing strategies for coupling fast simulation and interior-point optimization for applications such as: biomolecule design, nanophotonics, and optical semiconductor process inspection. Our approaches include using Hession-implicit methods in which the simulation and optimization occur in parallel [1] and strategies in which a detailed simulation model is used to generate a parameterized reduced order model [2,3,4]

REFERENCES:

[1]   Bardhan, J.P., J.H. Lee, M.D. Altman, S. Leyffer, S. Benson, B. Tidor, and J.K. White, "Biomolecule Electrostatic Optimization with an Implicit Hessian," Proceedings of Modeling and Simulation of Microsystems, pp. 164 -167, March, 2004.

[2]   Daniel, L. and J. White, "Numerical Techniques for Extracting Geometrically Parameterized Reduced Order Interconnect Models from Full-wave Electromagnetic Analysis," Proceedings of the IEEE AP-S International Symposium and USNC / URSI National Radio Science Meeting, June, 2004.

[3]   Lee, J.H., D. Vasilyev, A. Vithayathil, L. Daniel, and J. White, "Accelerated Optical Topography Inspection using Parameterized Model Order Reduction," forthcoming, Proceedings of the IEEE International Microwave Symposium, June, 2005.

[4]   Klemas, T., L. Daniel, and J. White, "Segregation by Primary Phase Factors: A Full-wave Algorithm for Model Orderreduction," forthcoming, Proceedings of the Design Automation Conference, Anaheim, CA, 2005.

Tools for Photonics in Integrated Circuit Design and Manufacturing

J.H. Lee, Y. Avniel, S. Johnson, J. White
Sponsorship: MARCO IFC, DARPA, NSF

Optical inspection, now the non-destructive, semiconductor process monitoring technique of choice, requires the solution of an inverse scattering problem to infer geometry from measured light. We have developed a new approach to accelerating this inverse scattering problem based on using parameterized model reduction [1]. The problem of analyzing optical effects in wavelength-sized structures also arises for developers of integrated nanophotonics, which is emerging as an important new technology. Nanophotonic designers have very few available tools, and we are beginning a project to improve the situation. We are developing approaches that can be used to extract circuit-level models of photonic devices [2,3] and are also developing new techniques for assessing the impact of roughness on the loss in photonic channels [4].

REFERENCES:

[1] Lee, J.H., D. Vasilyev, A. Vithayathil, L. Daniel, and J. White, "Accelerated Optical Topography Inspection Using Parameterizedmodel-order Reduction," forthcoming, Proceedings of the IEEE International Microwave Symposium, June, 2005.

[2] Klemas, T., L. Daniel, and J. White, "Segregation by Primary Phase Factors: A Full-wave Algorithm For Model-order Reduction" forthcoming, Proceedings of the Design Automation Conference, Anaheim, CA, 2005.

[3] Klemas, T., L. Daniel, and J. White, "A Fast Full-wave Algorithm to Generate Low-order Electromagnetic Scattering Models," forthcoming International Symposium on Antennas and Propagation and USNC/URSI National Radio Science Meeting, Washington, DC, July, 2005.

[4] Zhu, Z., A. Demir, and J. White, "A Stochastic Integral Equation Method for Modeling the Rough Surface Effect on" Proceedings of the IEEE Conference on Computer-Aided Design, San Jose, November 2004.

Photonic Integrated Circuits for Ultrafast Optical Logic

A. Markina, R.D. Williams, G.S. Petrich, R. Ram, L.A. Kolodziejski
Sponsorship: DARPA

The aim of this project is to model and to produce a modular, monolithically integrated, all-optical logic unit cell capable of performing a complete set of Boolean operations at speeds of hundreds of gigabits per second. The basic structure consists of a balanced Mach-Zehnder interferometer with an (In,Ga)(As,P)-based semiconductor optical amplifier (SOA) in each arm, as shown schematically in Figure 1.

Modeling is used to develop the design rules, to identify tradeoffs, to determine fabrication tolerances, and to estimate the effects of imperfections in semiconductor processing on the device's performance. Beam propagation method simulations are used to model passive waveguides, multimode interference couplers, and asymmetric twin-waveguide structures. Finite-difference, time-domain simulations are used to estimate the reflections between the various components. Custom MATLAB scripts are being developed to assess tradeoffs in SOA performance and to work toward design rules that specifically address the design of the SOAs for switching applications. The challenge is to optimize the performance of each component even when all of the components are monolithically integrated on a photonic integrated circuit.

Fabrication processes are being developed to create the all-optical logic unit cell. The waveguide design calls for vertical integration of the passive waveguide and active elements. This integration is achieved by employing a taper coupler to transfer the optical mode between the lower passive waveguide and the upper active waveguide of the twin-waveguide structure. In addition to the optical logic unit cell, isolated components are being fabricated and tested to confirm the device design and the computer simulation results.
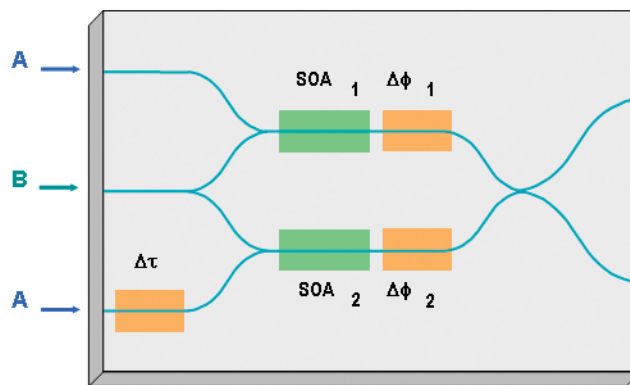

Figure 1: The optical logic unit cell. A balanced Mach-Zenhder interferometer composed of SOAs, multimode interference couplers, phase shifters and a time delay element.

Variation Analysis in Optical Interconnect

K. Balakrishnan, S. Staker, D. Boning
Sponsorship: MARCO IFC

The continual scaling of CMOS technology causes an increase in the amounts of systematic and random variation in circuits. Variation is also a concern in alternative optical interconnect approaches. In particular, both passive and active optical components can be affected by different sources of variation. In passive components such as waveguides and splitters, one source of variability tends to be of a geometric nature, causing uneven splitting ratios and overall transmission losses. For example, blurring across waveguide corners and bends can result in transmission losses. The sidewall roughness of a wave-guiding structure itself also contributes to non-negligible losses when a light source must travel a long distance from one end of a chip to another. In addition, temperature gradients within the chip as well as variation in the operating temperature of a chip can cause refractive index variations throughout these passive optical components. Current work being done in this area involves the analysis of effective-refractive-index variations on the transmission and splitting ratios of different splitter structures. These waveguide-splitter structures are as follows: High Transmission Cavity (HTC) splitter [1], Star-coupler design [2], and Uniform Bending Radius design [3]. Preliminary results have shown a sub-linear relationship between the refractive index variation and splitting losses for the HTC splitter. Figure 1 shows an example of an HTC splitter test structure, with the difference in color/shading representing the refractive index variations in the waveguide. Figure 2 illustrates results of both splitting ratio and transmission power as functions of index variation. Further work will examine other possible waveguide-splitting structures as well as analyze the effects of sidewall roughness caused by lithographic uncertainties on the robustness of wave-guiding structures.
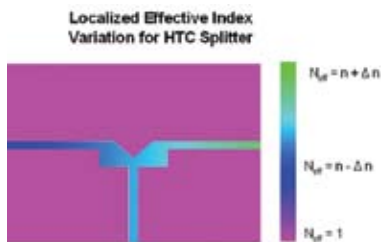

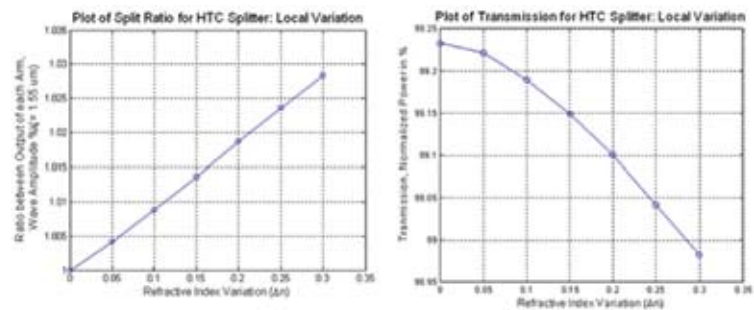Figure 1: Example HTC splitter test structure with a horizontal refractive-index gradient.

Figure 2: Simulation results of splitting ratio and transmission power versus refractive-index variation.

REFERENCES:

[1] Manolatou, C., S.G. Johnson, S. Fan, P.R. Villeneuve, H.A. Haus, J.D. Joannopoulos, "High-Density Integrated Optics," *J. Lightwave Tech.,* 17(9) September 1999.

[2] Cassan, E., S. Laval, S. Lardenois, A. Koster, "On-chip Optical Interconnects with Compact and Low-loss Light Distribution in Silicon-on-Insulator Rib Waveguides," *IEEE J. Select Topics in Quantum Electronics,* 9(2), 460-464, Mar/Apr. 2003.

[3] Zheng, J.-F., F.H. Robertson, E. Mohammed, I. Young, D. Ahn, K. Wada, J. Michel, L.C. Kimerling, "On-chip Optical Clock Signal Distribution," *Optical Society of America.* 4(4), 254-258, 2003.

Trimming of Microring Resonators

D.K. Sparacin, J.P. Lock, C. Hong, K.K. Gleason, L.C. Kimerling, J. Michel
Sponsorship: NSF MRSEC, ISN

Microring resonators are basic building blocks of photonic circuits, enabling complex functionality for optical systems. However, as micro-ring resonator diameters shrink to less than 10 µm, non-deterministic pattern-transfer errors limit dimensional precision and preclude the fabrication of identical devices across an entire wafer. Thus, the ability to precisely trim microring resonators becomes increasingly important. Microring trimming is typically done by thermal methods, where a heater, integrated onto the microphotonic chip, modifies the effective index and thus the resonance condition of the ring. This architecture adds several fabrication steps, limits the density of devices to maintain thermal isolation, and requires significant power consumption to keep the rings "trimmed". Alternatively, we use an organo-silicon polymer film as a cladding material, in which the refractive index is adjusted via photo-oxidation when irradiated with ultraviolet light (Figure 1). Photo-oxidation decreases the refractive index of PECVD 6M2S by nearly 4%, from n=1.52 to n=1.46, enabling large resonance shifts that are not feasible with thermal trimming techniques. In this work, Si_3N_4 (n=2.2) waveguides, designed for single mode operation at λ = 1550 nm, were fabricated from a 0.4-µm Si_3N_4 film deposited onto a 3-µm oxide under-cladding layer on (100) Si. The Si_3N_4 was patterned using a polysilicon hard mask and 365-nm photolithography. The micro-rings have a diameter of 100µm and the Si_3N_4 waveguides have cross-sectional dimensions of 400×750 nm². Afterwards, an organo-silicon top cladding layer was deposited directly onto the ring resonator devices using a PECVD process [1]. Spectral characterization of the microrings was done at the ring's through-port in both TE and TM polarizations by a C+L band, JDS Uniphase swept wavelength system (tunable laser and broadband photodetector) used in conjunction with a Newport Auto-Align System. Resonance shifts (Figure 2) from the Si3N4 rings were as large as 12.8 nm for the TE mode and 23.5 nm for the TM mode. Experimental results were compared with shifts predicted by theory. As a quick, localized, and controllable technique to produce large and precise resonance shifts, photo-oxidation trimming provides an attractive alternative to conventional trimming techniques.
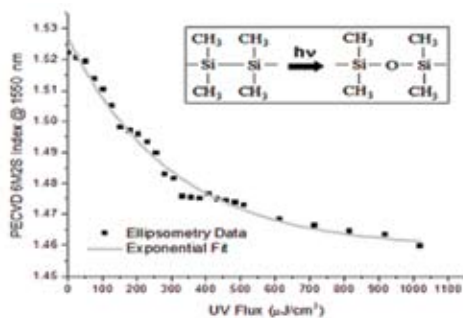

Figure 1: The refractive index of PECVD 6M2S cladding material decreases with UV irradiation as a result of photo-oxidation. The inset depicts the photo-oxidation reaction.
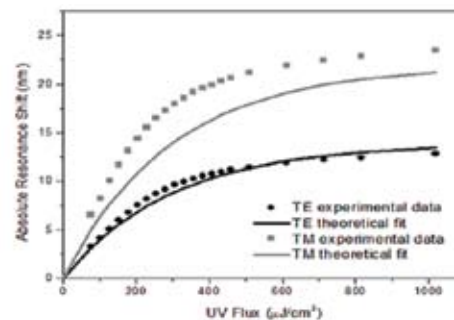

Figure 2: The experimental resonance shifts for TE and TM polarizations are compared with modeled results.

REFERENCE

[1] Lock, J.P., K.K. Gleason, "Tunable Waveguides via Photo-oxidation of Plasma-polymerized Organo-silicon Films," *Applied Optics*, Vol 41, pp. 1691-1697, 2005.

Optical Gain Media

L. Dal Negro, M. Stolfi, J. Michel, X. Duan, S. Saini, L.C. Kimerling, J. LeBlanc, J. Haavisto
Sponsorship: Charles Stark Draper Laboratories

The recent discovery of efficient energy-transfer between silicon nanocrystals (Si-nc's) and erbium (Er) ions has initiated an entirely new approach that profits from the advantages of quantum size effects and silicon (Si) rare earth doping, promising a route towards the integration of CMOS technology with 1.54-µm light sources. Despite several exciting breakthroughs, the nucleation of efficient light-emitting Si-nc generally requires annealing temperatures in excess of 1000 °C, severely limiting CMOS-compatibility. However, very recently Franzò [1] et al. demonstrated that Er-sensitization can occur at temperatures as low as 800°C, stimulating a debate on the ultimate nature of the energy transfer process.

We have recently fabricated erbium-doped, silicon-rich SiO_2 (Er:SRO) slab waveguides on Si substrates by reactive, radio-frequency (RF) magnetron-sputtering followed by thermal annealing. By studying Er emission versus Er:SRO annealing temperature, we found that the emission intensity is maximized between 600°C and 700°C for a Si content of 38% at. For samples annealed at 600°C, we are currently investigating the presence of light amplification and optical gain through variable stripe length (VSL) measurements.

These Er:SRO films can be used for the fabrication of compact waveguide optical amplifiers and integrated light sources with full CMOS-compatibility.
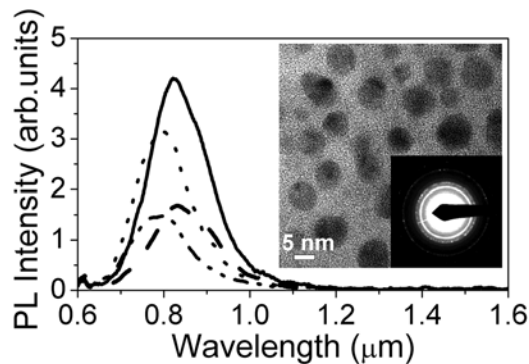

Figure 1: Room temperature PL spectra of Si-nc in SiO_2 samples without Er with different silicon content annealed at 1100 °C for 1 hour in a N_2 atmosphere. The Si contents for the samples are: 34 at% (dash-dot line), 35 at% (dotted line), 38 at% (solid line) and 43 at% (dash line). (inset) Plan-view TEM image and electron diffraction pattern for the Si-nc sample with 38 at% Si. [2]
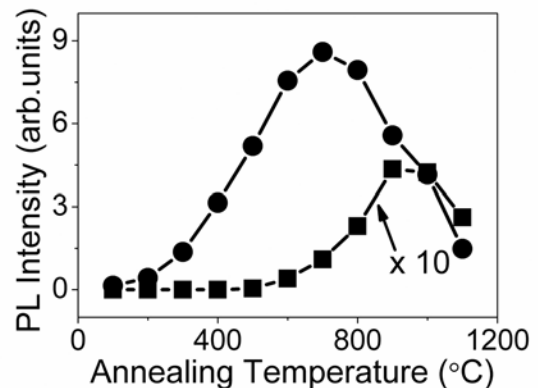

Figure 2: Room-temperature Er emission versus annealing temperature for Er in SiO_2 containing Si-nc samples with 38 at% Si and Er concentration of 8.2 x 10^{19} cm^{-3} (circles) and Er in SiO_2 samples with Er concentration of 9 x 10^{19} cm^{-3} (squares, magnified by 10). [2]

REFERENCES:

[1]   Franzò, G., S. Boninelli, D. Pacifici, F. Priolo, F. Iacona, and C. Bongiorno, *Appl. Phys. Lett.*, 82, 3871 2003.

[2]   Stolfi, M., L. Dal Negro, J. Michel, X. Duan, J. LeBlanc, J. Haavisto, and L.C. Kimerling, *MRS Proceedings*, 832 F11.8 2005.

Silicon Waveguide Structures

D.K. Sparacin, S.J. Spector, L.C. Kimerling
Sponsorship: NSF-MRSEC

The silicon/silicon-dioxide materials platform (Si-SiO_2) is ideal for microphotonics due its high index of refraction difference between the waveguide core and cladding (Δn), CMOS-fabrication compatibility, and process knowledge-base. Additionally, the Si-SiO_2 system allows for optoelectronic functionality, unlike other competing high Δn, dielectric-based, CMOS-compatible, materials systems. While the properties of the Si-SiO_2 system are attractive, they are not fully realized when waveguides are fabricated. For silicon waveguides, nm-scale sidewall roughness is the prime cause of transmission loss and an impediment to use. Oxidation of rough silicon surfaces is an effective method of smoothing silicon and can enable high transmission waveguides. However, oxidation smoothing is typically performed by high-temperature annealing in an oxygen-rich environment. This process works well for smoothing silicon waveguide surfaces but lacks control in maintaining cross-sectional waveguide dimensions due to the large consumption of silicon during the oxidation process. In efforts to solve these deficiencies associated with oxidation

smoothing, we developed a new, more efficient silicon waveguide sidewall smoothing process using wet chemical oxidation. In this work we used a post-etch, multi-stepped approach for efficient smoothing (in terms of roughness amplitude reduction to material consumption) of patterned SOI waveguides. Wet chemical oxidation reduces waveguide transmission loss without sacrificing dimensional integrity or thermal budget. The use of common chemical oxidants, such as those used in wafer-cleaning processes, is ideal for this oxidation-smoothing technique. Transmission loss data was determined by the Fabry-Perot technique. As shown in Figure 1, the transmission loss is reduced, when compared to the as-fabricated data, for the different wet chemistries. The effect is strongest for the thinnest waveguides, where transmission loss is most sensitive to sidewall roughness. In this proof of concept work, we have reduced Si waveguide sidewall loss from 9.2 to 1.9 dB/cm.
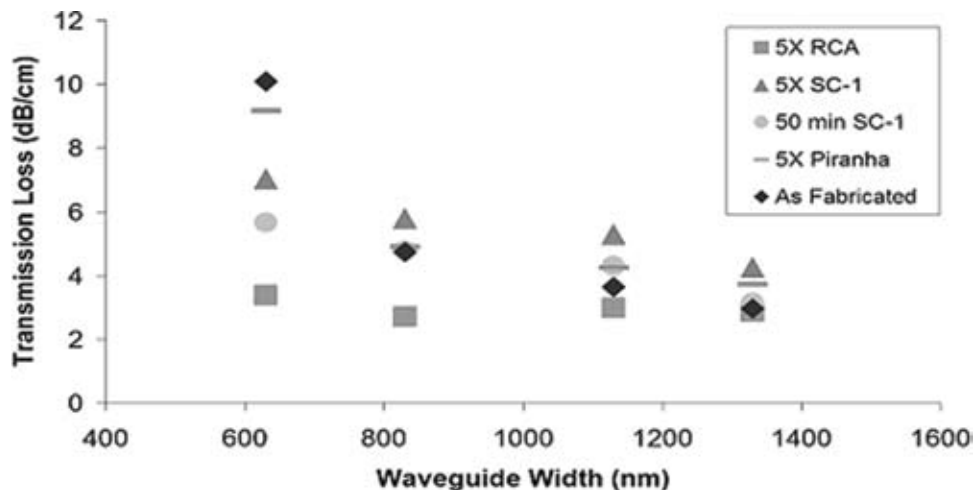

Figure 1: Transmission loss versus silicon waveguide width for various wet chemical oxidations. Measurement error bars for each data point (± 1 dB/cm) have been omitted for clarity. The waveguide height is 220 nm.

Sputtered Silicon Oxynitride for Silicon Microphotonics

J.G. Sandland, A. Eshed, S. Akiyama, S. Saini, V. Nguyen, L.C. Kimerling

Silicon oxynitride (SiON) is an ideal microphotonics waveguide material providing tunable control in composition nd refractive indices. SiON can be varied in refractive index from silicon dioxide values (n=1.46) to silicon-rich silicon nitride values (n~2.3) (Figure 1). This flexibility in refractive index enables optimization of the device's performance by executing trade-offs between the advantages of low-index contrast systems (low scattering loss and easy fiber-to-waveguide coupling) and high-index-contrast systems (small waveguide size and tight bending radii).

Sputter-processing has been investigated as a thin-film deposition alternative to traditional CVD-processing. Two room-temperature SiON sputter processes have been explored: co-sputtering of silicon oxide and silicon nitride targets and reactive sputtering from a silicon nitride target in an oxygen ambient environment. Process models were created and validated to predict refractive index and composition in both the reactive and co-sputtered depositions. Co-sputtered deposition was found to follow a mixture model, while reactive-sputter deposition was found to be either Si-flux limited or O-flux limited, depending on the partial pressure of oxygen in the reaction chamber and the power applied to the silicon nitride target (Figure 2). A study of materials composition, using SIMS showed sputtered SiON to be a homogeneous material with accurate control of refractive index. Reactively sputtered SiON was found to be Si-rich.

These sputtered materials were investigated for use as passive waveguides and active erbium-doped (Er) waveguide amplifiers. Losses below 1 dB/cm were observed for co-sputtered deposition (n=1.65) waveguides. Photoluminescence studies of Er-doped material showed lifetimes comparable to commercial EDFA material for both co-sputtered SiON and sputtered silicon dioxide. Dangling bonds from silicon were found to contribute both to waveguide-transmission loss and to non-radiative de-excitation in Er-doped materials.
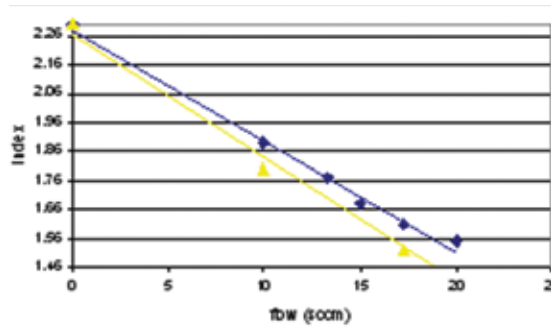

Figure 1: Theoretical prediction and experimental measurement of refractive index versus gas flow rate (10% O_2 in Ar) at 400W and 500W biased silicon nitride target power. (▲= 500 W, ◊ = 400W)
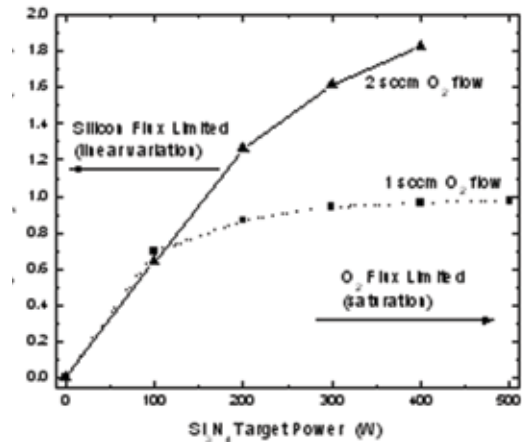

Figure 2: Gettered oxygen content versus silicon nitride target power, for 1 sccm and 2 sccm of O_2 gas flow. At high powers, the gettering rate of oxygen into the depositing film saturates, making the SiON film compositions easily tunable by adjustment of the O_2-flow rate. Solid lines are provided to guide the eye.

Modulators

S. Jongthammanurak, J. Liu, C-Y. Hong, J. Michel, K. Wada, D. Pan, L.C. Kimerling
Sponsorship: Pirelli Labs

Silicon microphotonics has drawn great interest for use in high-capacity data transfer using lightwave based technology. The Giga bit-per-second capacity data transfer in planar structures enables solutions for interconnects delay in computers. The wavelengths used in silicon microphotonics of 1.3 and 1.55 μm enable the telecommunication applications such as Local Area Networks (LANs) and fiber-to-the-Home (FTTH). Compatibility with existing complementary metal-oxide-semiconductor (CMOS) technology provides processing capability and enables the integration between microphotonics and silicon-based microelectronics.

Silicon-based optical modulators are crucial components that manipulate optical signals in the integrated microphotonics. At present, carrier related effect limits the speed of silicon-based modulators to only Gigahertz. High-speed application (> 10GHz) requires modulation based on field effect. In this work,

we study the field-effect based absorption modulation in pure germanium and germanium-rich silicon-germanium epitaxial films. Using spectral responsivity measurement, we relate the material absorption coefficients to spectral responsivity.

We observed the electro-absorption effect in germanium p-i-n diodes. For the energy lower than the bandgap (0.79 eV), the spectral responsivity is enhanced by the applied field. Above the band gap, we observed the Franz-Keldysh oscillation in spectral responsivity. This oscillation is due to band structure perturbation from the electric field. In Ge-rich, SiGe p-i-n diodes, we observed decreasing material absorption between direct and indirect band edges under the applied field using spectral responsivity by a laser source. The cause of this effect is being investigated. These materials are potential candidates for using as field-effect-based optical modulators in silicon microphotonics.
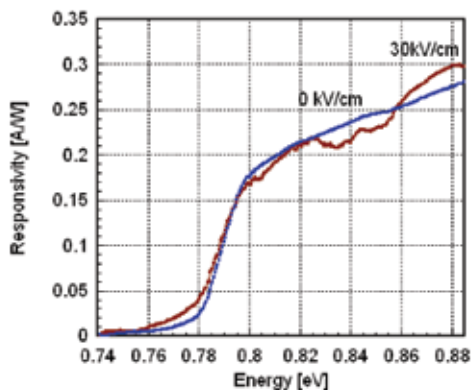

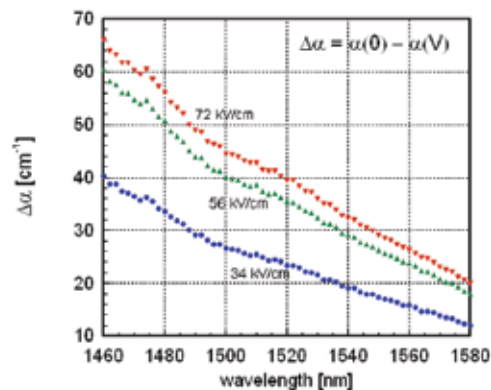Figure 1: Spectral responsivity from Ge p-i-n diodes under 0 kV/cm and 30kV/cm.

Figure 2 : Differences in Ge-rich SiGe absorption coefficients under the applied fields.

Fiber-Waveguide Coupling for HIC

V. Nguyen, T. Montalbo, C. Manolatou, A. Agarwal, J. Michel, L.C. Kimerling
Sponsorship: Analog Devices, Inc.

Integrated optical circuit designs seek to incorporate several optical functions on a single semiconductor chip. However, there is a need to couple signals from optical fibers to the on-chip waveguides and vice versa. Direct coupling results in high power-loss from three sources: reflections due to the difference in refractive index of the core materials, a mode-size mismatch between fiber and waveguide, and a mode-shape mismatch between a fiber's circular and waveguide's elliptical mode fields.

In this work, we explore an on-chip coupler to transform light from a single-mode optical fiber to a single-mode waveguide fabricated entirely by CMOS-compatible processes in MTL. In the vertical direction, the fiber mode diameter is reduced by a stack of varying refractive index layers formed on a cladding layer [1]. The layers, silicon oxynitride deposited by plasma enhanced chemical vapor deposition (PECVD), gradually increase in refractive index from top to the lower waveguide layer on oxide cladding on a silicon substrate. The lateral mode field conversion is completed with a linear taper and lens at the input facet [1, 2]. Both the lens and the tapered shape of the stack are defined through plasma etching.

The efficiency of the above fiber-to-waveguide coupling scheme has been measured and plotted as function of coupler length, input lens radius, and widths of input and output facets. The results are to supplement and correct the theoretical simulations of such structures with beam propagation (BPM) and finite-difference, time-domain (FDTD) methods.
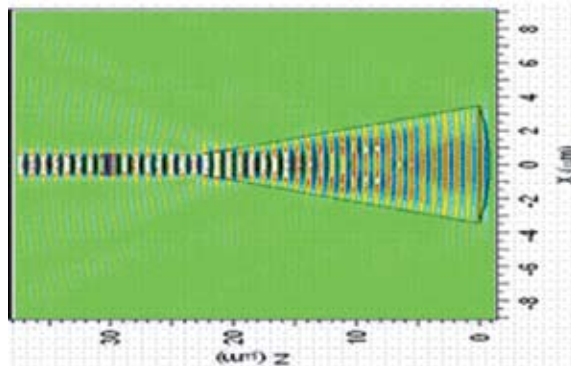

Figure 1: An FDTD simulation shows power--mode conversion to waveguide with a lens and taper combination.
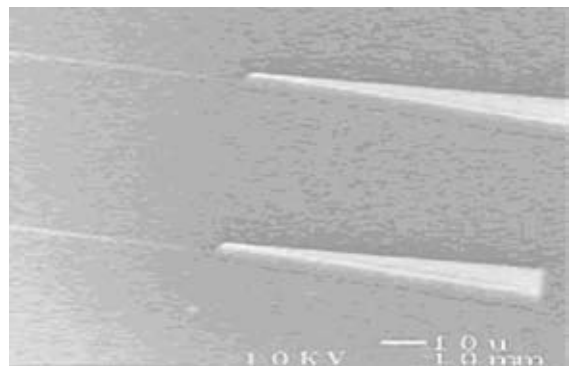

Figure 2: SEM shows 2 fabricated SiON--coupler structures on silicon.

REFERENCES:

[1]   Manolatou, C., "Passive Components for Dense Optical Integration Based on High Index Contrast" *[dissertation]* Cambridge (MA): MIT, 2001, pp 127-150 of 182. [Available from: Barker Libraries Microforms, MIT, Cambridge (MA); Thesis E.E. 2001 PhD]

[2]   Montalbo, T., "Fiber to Waveguide Coupler for Silicon Photonics" *[dissertation]* Cambridge (MA): MIT, 2004, pp 39-52 of 82. [Available from: Barker Libraries Microforms, MIT, Cambridge (MA); Thesis DMSE 2004 MS]

Novel Waveguide Electro-absorption Modulators for Optical Interconnects Utilizing an Insulator/Semiconductor/Insulator Structure

C.L. Dohrman, S. Gupta, R.J. Ram, E.A. Fitzgerald
Sponsorship: MARCO IFC, BAE

We are developing a novel microphotonic device to modulate light intensity in waveguides and photonic integrated circuits. The device is a type of electro-absorption modulator that uses the well-known quantum-confined Stark effect, which causes the absorption spectrum of an ultra-thin semiconductor layer to shift to lower energies with the application of an electric field. The device differs from existing electro-absorption modulators in two important ways. First, it uses an insulator/active, region/insulator structure instead of the semiconductor/quantum well/semiconductor structure used in existing electro-absorption modulators (Figure 1). Second, it uses an amorphous, nanocrystalline, or monocrystalline wafer-bonded quantum-confined active region instead of the epitaxially deposited quantum-confined active region used in existing devices. In addition, we have discovered four methods to suppress absorption saturation and voltage screening in our new device. This suppression is accomplished by decreasing the recombination lifetime of electron-hole pairs in the active region by (i) decreasing the thickness of the active region to prevent charge separation and to increase the ratio of interface to active volume, (ii) increasing the concentration of interface states at the interface of the quantum well and insulator by modifying the cladding material, (iii) adding to the active region of impurities (such as gold) that act as recombination centers , or (iv) adding to the active region of network modifiers (such as nitrogen) that increase the concentration of dangling bonds.
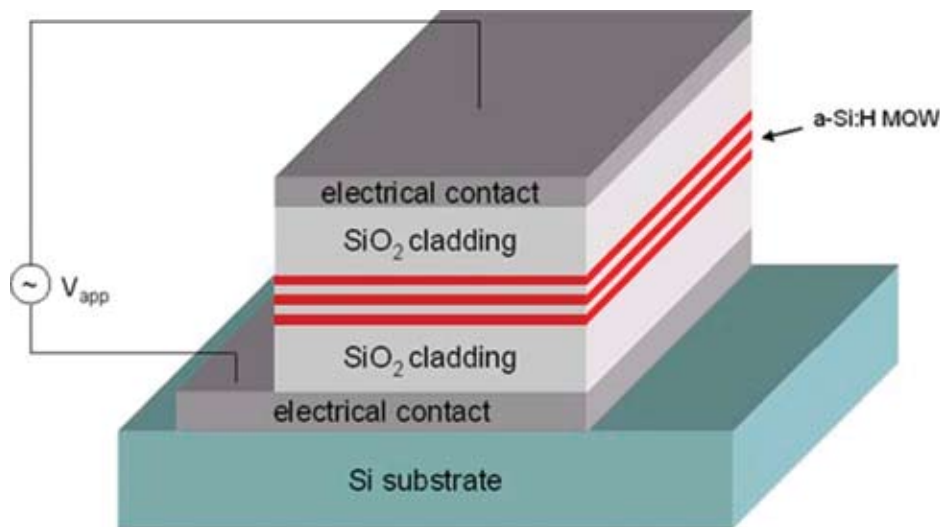

Figure 1: Schematic of insulator/semiconductor/insulator structure of electro-absorption modulator under development.

Faraday Rotation in Semiconductors for Photonic Integration

T. Zaman, X. Guo, R.J. Ram
Sponsorship: DARPA

The demonstration of waveguide isolators and circulators that can easily be integrated with active and passive optical components is essential to large-scale photonic integration. Indium Phophide (InP) is a widely used substrate for photonic components. Thus an InP-based waveguide isolator will provide the possibility for large-scale photonic integration. Iron (Fe)-doped InP with an Fe concentration of 2.9×10^{16} cm^{-3} was measured for its Faraday effect. At 1550 nm, the Verdet coefficient is 23.8 °/cm/T and the absorption coefficient is 0.20 cm^{-1}. The result shows that achieving isolation in acceptable length waveguides (~500um) is possible with improved Fe-doping concentration (~ 10^{18} cm^{-3}).

In order to rotate the polarization state of light within a waveguide, the Faraday material must be incorporated within a zero-birefringence waveguide. High-index contrast waveguides where the geometric birefringence is eliminated, have been demonstrated [1-2]. Deeply etched InP waveguides, as shown in Figure 2, with zero-birefringence and low optical loss have been demonstrated. In summary, the most significant materials challenges have been overcome for the realization of fully integrated waveguide optical isolators.
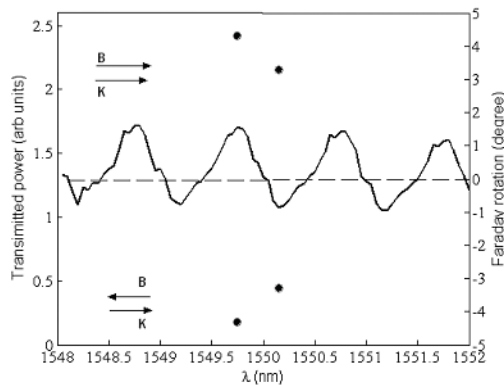

Figure 1: The dots indicate the rotation angle for linear polarization upon transmission through a InP/InGaAsP/InP resonator with an Fe concentration of 1×10^{17} cm^{-3} grown on a 300-μm InP substrate with an Fe concentration of 1×10^{16} cm^{-3}. For reference, the power transmission spectrum is also shown.
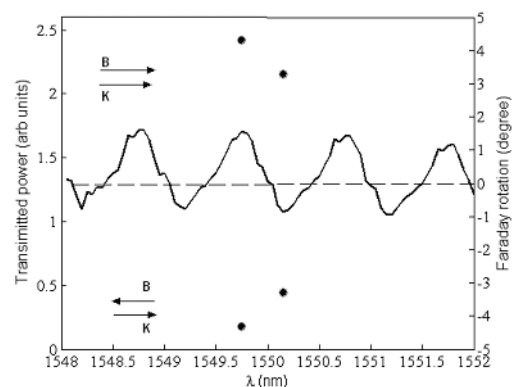

Figure 2: Waveguide width vs. wavelength to achieve zero birefringence.

REFERENCES:

[1]   Wolfe, R., J. Hegarty, J. F. Dillon, Jr., L.C. Luther, G.K. Celler, L. E. Trimble, and C. S. Dorsey, "Thin-film Waveguide Magneto-optic Isolator," *Appl. Phys. Lett.,* 46(9), pp. 817-819. 1985.

[2]   Watts, M.R., S. G. Johnson, H. A. Haus, and J.D. Joannopoulos, *Opt. Lett.* 27(20), pp. 1785-1787, 2002.

Slice-and-cascade Simulation of 3-D Optical Systems

Z. Xu, G. Barbastathis, in collaboration with M.A. Neifeld (University of Arizona)
Sponsorship: Laboratory of 3D Optical Systems

Understanding the Bragg selectivity requires getting an accurate prediction of the diffraction field of a volume hologram. So far, several methods have been introduced to analyze the diffraction property of volume hologram. One popular method is the Coupled Wave Theory (CWT), which was first applied to holography by Kogelnik. His classic paper presents an elegant expression of the diffraction efficiency by considering coupling of the 0th and 1st diffraction orders. The drawback of CWT is the limitation for complicated fringe shapes. An alternative is the so-called Born approximation theory. Though this method gives an analytic result for the diffraction field and can be applied to arbitrary geometry of hologram, it is valid only under the first-order approximation which means weak refractive index modulation.

In 3-D imaging systems, we usually utilize the spherical wave-recorded holographic element and pursue a maximum efficiency. This requires us to choose the hologram with complicated geometry and strong modulation. To model and optimize such holograms, we have developed a novel numerical method called slice-and-cascade simulation for the problem of diffracting volume holograpic. The idea is to decompose the thick element into slices and calculate the propagation slice by slice. Intuitively, we can think the propagation in one slice as following: firstly light is translating in a homogeneous space and then is modulated by a phase grating. Also, based on this assumption, we can get a recursive relation of the fields between two adjacent slices.

Figures 1 and 2 show a very good agreement of our method with the CWT, verifying that the method works well in the well-known plane-wave hologram case. We are currently in the process of extending the slice-and-cascade method to the more complicated geometry of interest, and we are optimizing our system design.
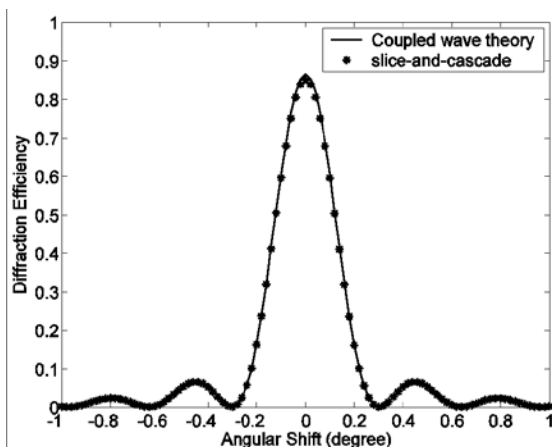

Figure 1: comparison of slice-and-cascade method with CWT as angular selectivity for plane-to-plane volume hologram
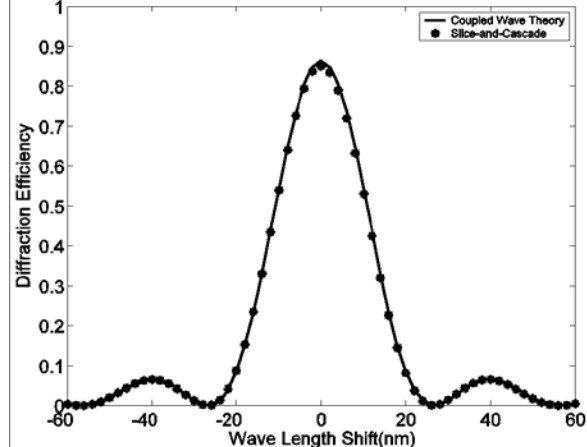

Figure 2: comparison of slice-and-cascade method with CWT as wavelength selectivity for plane-to-plane volume hologram

REFERENCES:

[1]   Kogelnik, H., "Coupled Wave Theory for Thick Hologram Gratings," *Bell Syst. Tech. J.*, 48(9), 1969, pp. 2909-2947.